Invited Review Article

Overview of the search for signs of space weathering on the low-albedo asteroid (101955) Bennu

B.E. Clark [a,*], A. Sen [a], X.-D. Zou [b], D.N. DellaGiustina [c], S. Sugita [d], N. Sakatani [e], M. Thompson [f], D. Trang [g], E. Tatsumi [d], M.A. Barucci [h], M. Barker [i], H. Campins [j], T. Morota [k], C. Lantz [l], A.R. Hendrix [b], F. Vilas [b], L. Keller [m], V.E. Hamilton [n], K. Kitazato [o], S. Sasaki [p], M. Matsuoka [q], T. Nakamura [q], A. Praet [h], S.M. Ferrone [h], T. Hiroi [r], H.H. Kaplan [i], W.F. Bottke [n], J.-Y. Li [b], L. Le Corre [b], J.L. Molaro [b], R.-L. Ballouz [c], C.W. Hergenrother [s], B. Rizk [c], K.N. Burke [c], C.A. Bennett [c], D.R. Golish [c], E.S. Howell [c], K. Becker [c], A.J. Ryan [c], J.P. Emery [t], S. Fornasier [h], A.A. Simon [i], D.C. Reuter [i], L.F. Lim [i], G. Poggiali [h], P. Michel [u], M. Delbo [u], O.S. Barnouin [v], E.R. Jawin [n], M. Pajola [w], L. Riu [q], T. Okada [q,v], J.D.P. Deshapriya [x], J.R. Brucato [y], R.P. Binzel [z], D.S. Lauretta [c]

[a] Department of Physics and Astronomy, Ithaca College, Ithaca, NY, USA
[b] Planetary Science Institute, Tucson, AZ, USA
[c] Lunar and Planetary Laboratory, University of Arizona, Tucson, AZ, USA
[d] The University of Tokyo, Tokyo, Japan
[e] Rikkyo University, Tokyo, Japan
[f] Purdue University, West Lafayette, IN, USA
[g] University of Hawaii at Manoa, Honolulu, HI, USA
[h] LESIA, Observatoire de Paris, Université Paris Cité, Université PSL, CNRS, Sorbonne Université, Meudon, France
[i] NASA Goddard Space Flight Center, Greenbelt, MD, USA
[j] University of Central Florida, Orlando, FL, USA
[k] Nagoya University, Nagoya, Japan
[l] Institut d'Astrophysique Spatiale, Université Paris-Saclay, CNRS, 91405 Orsay, France
[m] ARES, NASA Johnson Space Center, Houston, TX, USA
[n] Southwest Research Center, Boulder, CO, USA
[o] The University of Aizu, Fukushima, Japan
[p] Osaka University, Suita, Japan
[q] Institute of Space and Astronautical Science (ISAS), Japan Aerospace Exploration Agency (JAXA), Sagamihara, Japan
[r] Brown University, Providence, RI, USA
[s] Ascending Node Technologies, Tucson, AZ, USA
[t] Northern Arizona University, Flagstaff, AZ, USA
[u] Université Côte d'Azur, Observatoire de la Côte d'Azur, CNRS, Laboratoire Lagrange, Nice, France
[v] Applied Physics Laboratory, Johns Hopkins University, Laurel, MD, USA
[w] INAF, Observatory of Padova, Italy
[x] INAF, Observatory of Rome, Italy
[y] INAF, Arcetri Observatory, Florence, Italy
[z] Massachusetts Institute of Technology, Cambridge, MA, USA

ARTICLE INFO

ABSTRACT

This paper summarizes the evidence for the optical effects of space weathering, as well as the properties of the surface that control optical changes, on asteroid (101955) Bennu. First, we set the stage by briefly reviewing what was known about space weathering of low-albedo materials from telescopic surveys, laboratory simulations, and sample return analysis. We then look at the evidence for the nature of space weathering on Bennu from recent spacecraft imaging and spectroscopy observations, including the visible to near-infrared and thermal infrared wavelengths, followed by other measurements such as normal albedo measurements from LIDAR scans. We synthesize these different lines of evidence in an effort to describe a general model of

---

* Corresponding author.
  E-mail address: bclark@ithaca.edu (B.E. Clark).

space weathering processes and resulting color effects on dark C-complex asteroids, with hypotheses that can be tested by analyzing samples returned by the mission.

A working hypothesis that synthesizes findings thus far is that the optical effects of maturation in the space environment depend on the level of hydration of the silicate/phyllosilicate substrate. Subsequent variations in color depend on surface processes and exposure age. On strongly hydrated Bennu, in color imaging data, very young craters are darker and redder than their surroundings (more positive spectral slope in the wavelength range 0.4–0.7μm) as a result of their smaller particle sizes and/or fresh exposures of organics by impacts. Solar wind, dehydration, or migration of fines may cause intermediate-age surfaces to appear bluer than the very young craters. Exposed surfaces evolve toward Bennu's moderately blue global average spectral slope. However, in spectroscopic and LIDAR data, the equator, the oldest surface on Bennu, is darker and redder (wavelength range 0.55–2.0μm) than average and has shallower absorption bands, possibly due to dehydration and/or nanophase and/or microphase opaque production.

Bennu is a rubble pile with an active surface, making age relationships, which are critical for determining space weathering signals, difficult to locate and quantify. Hence, the full story ultimately awaits analyses of the Bennu samples that will soon be delivered to Earth.

1. Introduction

1.1. Scope of this review

Spatially resolved in situ remote sensing studies of the low-albedo, carbonaceous (C-complex, B-type) asteroid, (101955) Bennu were carried out by the OSIRIS-REx spacecraft (Lauretta et al., 2017, 2021). This review seeks to assemble the spacecraft observations together with possible explanations into a single self-consistent story about the nature of space weathering on this asteroid. Because space weathering processes can cause optical changes that impede our ability to understand reflected light spectral measurements, we are interested in knowing how/if space weathering effects manifest on dark asteroids in general, and on Bennu in particular. OSIRIS-REx is an asteroid sample return mission, providing an invaluable opportunity for us to ground-truth the returned samples against interpretations of the remote observations of their source body.

What is space weathering? The term "space weathering" refers to the chemical and physical changes that occur when an airless body is exposed to solar wind and micrometeoroid impacts. These processes result in many time-dependent changes to the properties of a surface and can thus be used to determine a surface's exposure age (Section 1.5). The study of space weathering first came into focus when it was noted that lunar craters change in albedo over time (Gold, 1955). Excellent summaries of lunar space weathering are presented in Hapke (2001) and Pieters et al. (2000). More recently, space weathering principles have been applied to the study of bright stony (S-type) asteroids (e.g. Clark et al., 2002; Gaffey, 2010). The OSIRIS-REx spacecraft encounter with Bennu and the Hayabusa2 spacecraft encounter with (162173) Ryugu have extended our understanding of space weathering effects to C-complex asteroids, although the low albedo makes signs of space weathering more challenging to interpret.

The study of the optical effects of space weathering includes not only spacecraft observations but also telescopic surveys and laboratory simulations. Laboratory simulations of space weathering use ion irradiation to simulate solar wind and pulsed-laser irradiation to simulate micrometeoroid impacts (Brunetto et al., 2015; Matsuoka et al., 2015; Lantz et al., 2018). In telescopic observations of asteroids, space weathering is investigated by statistical analyses of populations with shared spectral or dynamical properties (Lantz et al., 2013; Vernazza et al., 2009; Lazzarin et al., 2006; Nesvornỳ et al., 2005; Hendrix and Vilas, 2019).

Spectral continuum slope: This review is primarily concerned with the optical effects of space weathering, as well as the properties of the surface that control optical changes on Bennu. A major theme is the observation and interpretation of spectral continuum slope changes on Bennu in the context of space weathering. We first set the context for the observations of Bennu by briefly reviewing what was known about space weathering of low-albedo materials from telescopic surveys and laboratory simulations prior to the OSIRIS-REx encounter. We then look at the evidence for the nature of space weathering on Bennu from spacecraft imaging and spectroscopy observations (including the visible to near-infrared and thermal infrared wavelengths), as well as normal albedo measurements from LIDAR scans. Because the LIDAR data are obtained with an active light source, they are excellent probes of global-scale albedo patterns as demonstrated by Hemingway et al. (2015). We synthesize these different lines of evidence in an effort to distinguish a general model of space weathering processes and effects on dark C-complex asteroids.

Samples from Ryugu: At the time of this writing, the samples returned by the JAXA Hayabusa2 mission (Watanabe et al., 2017, 2019; Yada et al., 2022; Pilorget et al., 2022) to C-complex asteroid (1621730) Ryugu, a sister mission of OSIRIS-REx, are under study. The Ryugu results are also important to our understanding of space weathering on low-albedo asteroids, and hence we include a brief discussion of them in this paper. Evidence about the nature of space weathering on Ryugu and Bennu will be integrated to produce hypotheses that can be tested using the samples returned by the missions. The samples from Bennu and Ryugu will provide ground-truth of the microscopic, macroscopic, and spectroscopic effects of space weathering on these asteroids.

1.2. Previous telescopic and spacecraft studies of space weathering of low-albedo asteroids

The C-complex asteroids are thought to be the parent bodies of most or all carbonaceous chondrite meteorites (CCs). Their mineralogy is of great interest due to their prevalence in the asteroid regions of the Solar System. CCs are closer to the composition of our Sun than any other meteorites, and hence are considered to be some of the most primitive material available in our solar system. Among the CCs, CI chondrites are thought to be closest to solar nebular composition due to their higher content of volatile elements. CI and CM CCs are enriched in carbon (2.2–5.4 weight %) (Pearson et al., 2006), as compared with ordinary chondrites (<0.20 weight %) (Moore and Lewis, 1967). CCs are far less abundant in Earthly meteorite collections than the ordinary chondrites; however, there is good evidence for selection effects in passage through our atmosphere. Bennu is close in spectral properties to CI and CM meteorites (subtypes of CC meteorites) (Clark et al., 2011; Hamilton et al., 2019), being primarily composed of hydrated phyllosilicates (aqueously altered silicates) with an organic carbon-rich matrix. Most recently, however, Hamilton et al. (2022) found another, possibly better analog for Bennu: the unique meteorite CR1 Grosvenor Mountains (GRO) 95577 looks very Bennu-like in the thermal infrared wavelengths. Like Bennu and the CI and CM chondrites, CR meteorites can contain substantial amounts of H_2O and OH in addition to exotic organics.

Early results: To investigate the possible spectral signatures of exposure to the space environment on carbonaceous low-albedo asteroids, Lantz et al. (2013) studied the reflectance spectra of particulate

CC samples (assumed to represent asteroid subsurface materials) and compared them with telescopic spectra of asteroids (assumed to represent asteroid surface materials). The authors further assumed that primitive Ch/Cgh-type C-complex asteroids are the parent bodies of CMs based on the similarity in the wavelength position of an absorption feature at 0.7 μm. Lantz et al. (2013) then reasoned that differences between the laboratory spectra of the meteorites and the telescopic spectra of the asteroids' surfaces (wavelength range $0.4-2.5$ μm) could be due to differences in textural properties or exposure of the asteroids to space weathering. For the Lantz et al. (2013) study, meteorites were measured at a wide variety of particle size ranges, from <45 μm to <500 μm. Their results indicated that surface maturation leads to spectral bluing of asteroids, with little to no concurrent albedo change or band modification.

Asteroid families: However, different results came from studies by Kaluna et al. (2016) and Fornasier et al. (2016). These authors sought to parameterize the effects of space weathering by studying the ground-based spectra of the Themis and Beagle near-Earth asteroid families. The Beagle family has been independently shown (Nesvornỳ et al., 2008) to have been created when a larger Themis-family object was collisionally shattered into fragments; therefore, Kaluna et al. assumed that all of the asteroids in the study started from the same base mineralogy. This relationship means that the Beagle-family objects are younger than the Themis-family objects, allowing Kaluna et al. to attribute spectral differences between the families to space weathering. In particular, Kaluna et al. (2016) studied the spectral slope of telescopically obtained spectra and found that asteroids from the older Themis family have redder spectral slopes and lower albedos than asteroids from the younger Beagle family. This led the authors to conclude that space weathering among C-complex asteroids leads to darkening and spectral reddening. However, while the spectral color results of Kaluna et al. (2016) are statistically significant, the albedo results are much less so (see Fig. 7 in Kaluna et al. (2016)). Lazzarin et al. (2006) also found evidence that C-complex asteroids redden over time through a similar study, but prefaced that conclusion with a large uncertainty attributed to the small number of families studied. Nesvornỳ et al. (2005) found evidence contradictory to the Kaluna et al. and Lazzarin et al. studies mentioned above, concluding that spectral bluing occurs with age. Their result is consistent with Lantz et al. (2013) and is far more statistically significant than Kaluna et al. (2016) or Lazzarin et al. (2006), given their thorough use of the Sloan Digital Sky Survey. However, both Lazzarin et al. and Nesvornỳ et al. emphasized the relevance of compositional variations when interpreting space weathering signals.

Using data from the Sloan Digital Sky Survey Moving Object Catalog, Thomas et al. (2021) performed a study of spectral color as a function of asteroid diameter for nine C-complex families to constrain the possible visible wavelength effects of space weathering on carbonaceous asteroids. They found two spectral slope trends that were correlated with asteroid size, but most families (eight of nine) showed a reduction in spectral slope with increasing object size until a minimum slope value was reached whereupon the trend reversed to increasing slope with increasing size. This trend was also correlated with family distance from the Sun, pointing to space weathering as a possible cause.

The Ceres example: On the dwarf planet Ceres, the apparent association of relatively bright and blue ejecta deposits with geologically young impact craters suggests a possible reddening space weathering effect, although the mechanisms are almost completely unknown (e.g., Schmedemann et al. (2016), Schröder et al. (2017) and Stephan et al. (2017)). Ceres' young ejecta deposits are bluer and generally associated with slightly weaker hydroxyl bands at 2.7 μm and NH_4 bands at 3.1 μm than the global average (Ammannito et al., 2016; Stephan et al., 2019).

The Phobos example: A study by Ballouz et al. (2019) sought to explain a similar color dichotomy on Phobos, a carbonaceous moon of Mars. They found that the rate of surface motion is correlated with the blue-ness of the surface of Phobos. This correlation led (Ballouz et al., 2019) to posit that fine grains are carried away by the bulk flow of the surface. They show that the re-surfacing rate in the blue regions may be faster than the space weathering rate on Phobos.

The open question which then remains is how space weathering is expressed on carbonaceous surfaces with varying compositions and particle sizes, and over a multitude of timescales and orbital environments.

1.3. Previous laboratory studies of space weathering of carbonaceous materials

Simulating space weathering processes in the laboratory using experimental techniques has proven to be a useful way of exploring how these surface processes operate on carbonaceous asteroidal surfaces. These experiments provide important context for remote sensing observations made at Bennu and Ryugu and serve to prepare us for the analysis of the samples returned by the OSIRIS-REx and Hayabusa2 missions. Although laboratory experiments have simulated both major constituent space weathering processes – ion irradiation for solar wind exposure (e.g., Brunetto et al. (2014) and Lantz et al. (2015)) and pulsed-laser irradiation for micrometeoroid bombardment (e.g., Matsuoka et al. (2015) and Gillis-Davis et al. (2017)) – these methods have not been studied in operation together. Nevertheless, the results of these studies have provided insight into the surface evolution of Bennu and Ryugu over time and have illuminated how space weathering may affect the spectral properties of these bodies. Laboratory experiment results have also informed theoretical models of the optical effects of space weathering (Hapke, 2001; Trang and Lucey, 2019).

Solar wind simulations: The link suggested by Clark et al. (2011) between Bennu and CI/CM meteorites resulted in those meteorite types being the primary target substrates for laboratory alteration experiments. However, simulations of solar wind irradiation have been performed for a wide variety of CC samples (select CI, CM, CV, and CO meteorites and the ungrouped C2 meteorite Tagish Lake) and compositionally related substances (e.g., natural bitumens, serpentine group minerals). The majority of these experiments have focused on irradiation with H^+ and He^+ (some of the major constituents of the solar wind) at energies of $1 \, keV$ (Laczniak et al., 2019, 2021), $40 \, keV$ (Lantz et al., 2017), or higher (Lazzarin et al., 2006). These experiments have resulted in inconsistent spectral properties in the target samples, including bluer and brighter spectra (Vernazza et al., 2013; Lantz et al., 2017), mildly reddened spectra that may be darker or brighter (Keller et al., 2015; Laczniak et al., 2019, 2020; Nakamura et al., 2020; Nakauchi et al., 2021), and spectra which exhibit no significant changes (Brunetto et al., 2014; Lantz et al., 2015). The energy of the ion irradiation may be correlated with the type of spectral changes observed in the experimental samples (Nakauchi et al., 2021). Similar to solar wind irradiation, solar UV irradiation can also lead to changes in spectral slope. Irradiation with strong UV light for 312 h (equivalent to a few years at 1 AU from the Sun) darkened a sample of CM2 Murchison by 15% (Kaiden et al., 2019). Spectral modifications have also been linked to microstructural and chemical changes in the samples as a result of ion irradiation. Nanophase Fe (metallic iron) and Fe-S (troilite) particles have been proposed as the cause for reddened spectra (Keller et al., 2015; Laczniak et al., 2019, 2020), and carbonization (loss of H from hydrocarbon molecules resulting in larger aromatic molecules) is hypothesized to result in bluing and darkening, particularly for the CM chondrites (Moroz et al., 2004b; Lantz et al., 2017). Other observations of changes in organic functional group chemistry in ion-irradiated CCs include not only an overall reduction in the concentration of organics, but a possible resistance of aromatic molecules to breakdown (Laczniak et al., 2021). Nakamura et al. (2019) note that porosity of a sample plays an important role in determining the optical changes as a result of ion irradiation. They find that when prepared as a pressed pellet, a CI meteorite (Y 980115) becomes bluer and brightens; when exposed to the same conditions in chip form, the sample reddens, with

Table 1

Spectral and compositional summary of results of simulated solar wind bombardment experiments on various carbonaceous meteorites and related phases. In this table, np: nanophase; mp: microphase; Mag: magnetite; S: sulfide (troilite) including FeS and FeNiS; sap: saponite; serp: serpentine; Tagish: C2-ungrouped Tagish Lake meteorite; TEM: transmission electron microscopy. An asterisk indicates terrestrial samples (Nakamura et al., 2019; Lantz et al., 2017; Laczniak et al., 2021, 2019; Nakamura et al., 2020; Keller et al., 2015; Lantz et al., 2015; Lazzarin et al., 2006; Brunetto et al., 2014; Vernazza et al., 2013; Nakauchi et al., 2021).

| Experiment type | Conditions | | | | Optical response | | TEM study | | | | | |
Solar wind	Sample	Form	Ion	Energy	Slope	Albedo	npFe	mpFe	npMag	mpMag	npS	mpS
Nakamura et al. (2019)	CI	Pellet	He$^+$	20 keV	Bluer	Brighter						
Nakamura et al. (2019)	CI	Chip	He$^+$	20 keV	Redder	Unchanged						
Lantz et al. (2017)	CI	Pellet	He$^+$	40 keV	Bluer	Brighter						
Laczniak et al. (2021)	CM	Chip	H$^+$	1 keV	Redder	Unchanged	–	–	–	–	–	–
Laczniak et al. (2019)	CM	Chip	H^{2+}	2 keV	Redder	Unchanged						
Laczniak et al. (2021)	CM	Chip	He$^+$	4 keV	Redder	Brighter	X	–	–	–	–	–
Nakamura et al. (2020)	CM	Chip	He$^+$	4 keV	Redder	Darker						
Laczniak et al. (2019)	CM	Chip	He$^+$	4 keV	Redder	Darker						
Keller et al. (2015)	CM	Chip	He$^+$	4 keV	Redder	Darker	X	–	–	–	X	X
Nakamura et al. (2020)	CM	Chip	He$^+$	20 keV	Bluer	Brighter						
Nakamura et al. (2019)	CM	Chip	He$^+$	20 keV	Bluer	Brighter						
Lantz et al. (2015)	CM	Pellet	He$^+$, Ar$^+$	40 keV	Unchanged	Unchanged						
Lantz et al. (2017)	CM	Pellet	He$^+$	40 keV	Bluer	Brighter						
Lantz et al. (2017)	CO	Pellet	He$^+$	40 keV	Redder	Darker						
Lazzarin et al. (2006)	CO	Pellet	Ar^{2+}	400 keV	Redder	Darker						
Lantz et al. (2017)	CV	Pellet	He$^+$	40 keV	Redder	Darker						
Brunetto et al. (2014)	CV	Pellet	He$^+$, Ar$^+$	40 keV	Redder	Darker						
Lazzarin et al. (2006)	CV	Pellet	Ar^{2+}	400 keV	Redder	Darker						
Vernazza et al. (2013)	Tagish Lake	Pellet	He$^+$, Ar$^+$	4 keV	Bluer	Brighter						
Lantz et al. (2017)	Tagish Lake	Pellet	He$^+$	40 keV	Bluer	Brighter						
Nakauchi et al. (2021)	Sap*	Pellet	H$^+$	10 keV	Redder	Unchanged						
Nakauchi et al. (2021)	Serp*	Pellet	H$^+$	10 keV	Bluer	Darker						

negligible change in albedo. We summarize the spectral results and associated microstructural and chemical products from ion irradiation experiments in Table 1.

Studying the results of space weathering laboratory simulations, Brunetto et al. (2015) note that exposing a CV (Allende) to ion irradiation (solar wind) leads to the preferential loss of H from organics and increased aromaticity, accompanied by associated carbonization. They point out that these chemical effects redden and darken the reflectance spectrum of the matrix, while Moroz et al. (1998), in their study of ion irradiation of natural solid bitumen, also attribute spectral "flattening" (i.e. reduction of spectral band depth and decrease of band depth in absorption features) to the same process. Moroz et al. (1998) also suggest that this holds true for ion irradiation of organics in meteorite material. According to the Nakamura et al. (2019) study of CI and CM meteorite alteration, a reddening spectral change was noted with increasing total dose of ion irradiation, but only after some bluing had occurred at <0.65 μm wavelength. Nakauchi et al. (2021) report that absorption features in the 3 μm region were modified by hydrogen ion irradiation. Specifically, the absorption band area of the 2.8 μm band increased with hydrogen irradiation, indicating that the abundance of OH and/or H_2O increased in the reaction layer of the samples. However, Prince and Loeffler (2022) also found an increase in the OH band in laser irradiation of CM/CI simulant material. Since their process would not implant any hydrogen, it is therefore possible that the OH band increase is not due to H implantation, but to terrestrial water adsorption.

As is found by Laczniak et al. (2021), irradiation of Murchison samples with either He$^+$ or H$^+$ results in an increase of H_2O and OH$^-$. However, irradiation with H$^+$ leads to twice the magnitude of H_2O increase as compared to He$^+$. This dehydration/hydration phenomenon is supported by the findings of Nakauchi et al. (2021). Laczniak et al. (2021) suggest that the increase in H_2O by He$^+$ irradiation is from the amorphization of phyllosilicates leaving broken surface bonds, creating more sites at which adsorbed water can attach. In contrast, the increase in H_2O creation by H$^+$ irradiation may be due to decomposition of phyllosilicates and in situ water formation, e.g., H$^+$ combining with O to form OH and H_2O. Thus, when considering the effects of solar wind, the results of any study which uses only He+ ions must be considered in context since He+ irradiation cannot simulate every OH/H_2O process known to occur on C-complex surfaces.

Micrometeoroid bombardment simulations: In addition to solar wind irradiation, micrometeoroid bombardment has been simulated in the laboratory. These experiments have typically employed pulsed-laser irradiation for samples prepared either as rock chips or powders with various grain sizes. The target materials include many of the same samples as used in the ion irradiation experiments (CI, CM, CV, CO, C2-ungrouped Tagish Lake, and limited CK and Howardite samples), providing a point of comparison (Moroz et al., 2004a; Hiroi et al., 2013; Matsuoka et al., 2015, 2020; Gillis-Davis et al., 2017; Thompson et al., 2019, 2020). Laboratory experiments have used lasers of varying energies and shot numbers, with some simulating progressive space weathering via multiple rounds of irradiation (e.g., Matsuoka et al. (2015) and Thompson et al. (2020)). Similar to ion irradiation experiments, the spectral effects resulting from pulsed laser irradiation are inconsistent, with some samples exhibiting bluer and darker spectra (Matsuoka et al., 2015, 2020), while others become redder and darker (Moroz et al., 2004a; Prince and Loeffler, 2022). Analyses of the microstructural and chemical characteristics of these samples by Thompson et al. (2020) and Laczniak et al. (2021) revealed a diverse compositional population of nanoparticles, which include Fe-Ni-S (pentlandite), FeS (troilite), Fe (metallic iron), and some Fe-oxides (e.g., magnetite). The dominant mineralogy of these nanoparticles evolved over progressive irradiation (i.e., simulated exposure) in some experiments (Thompson et al., 2020; Laczniak et al., 2021), which may contribute to the inconsistency in spectral results; the composition of these nanoparticles may change with sustained exposure to interplanetary space. Laser-irradiated CCs have also shown an overall increase in detectable organics, particularly in aromatics of CMs (Thompson et al., 2020), and similar experiments for isolated organic species caused the formation of alkanes and alkenes (Ishikawa and Sato, 2020). Prince and Loeffler (2022) found that irradiation of CI and CM simulant material caused darkening, while the blue spectral slopes reddened until almost flat. They also found that laser irradiation caused the depth of the <3 μm absorption band to increase by as much as 30%. We summarize the spectral trends and associated microstructural and chemical products from pulsed-laser irradiation experiments in Table 2.

Another approach to constraining space weathering effects was led by Lantz et al. (2013). They found a bluing and brightening maturation effect which is strongest in the visible wavelengths. Subsequently, Lantz et al. (2017) found that anhydrous meteorites Allende (CV) and Lance

Table 2
Spectral and compositional summary of simulated micrometeoroid space weathering experimental results on various carbonaceous meteorites and related phases. Abbreviations and symbology are as in Table 1. (phyllo: phyllosilicates.) (Hiroi et al., 2013; Moroz et al., 2004a; Matsuoka et al., 2015, 2020; Thompson et al., 2020; Gillis-Davis et al., 2017; Kaluna et al., 2017; Prince and Loeffler, 2022).

Experiment type	Conditions			Optical response		TEM study					
Micrometeoroid impact	Sample	Form	Laser	Slope	Albedo	npFe	mpFe	npMag	mpMag	npS	mpS
Hiroi et al. (2013)	CI	Pellet	1064 nm	Bluer	Darker						
Hiroi et al. (2013)	CK	Pellet	1064 nm	Redder	Darker						
Moroz et al. (2004a)	CM	Powder	1064 nm	Redder	Darker						
Matsuoka et al. (2015, 2020)	CM	Powder	1064 nm	Bluer	Darker	–	–	–	–	X	X
Thompson et al. (2020)	CM	Chip	1064 nm	Bluer	Darker	X	–	X	–	X	X
Hiroi et al. (2013)	CM	Pellet	1064 nm	Bluer	Darker						
Hiroi et al. (2013)	CO	Pellet	1064 nm	Redder	Darker						
Gillis-Davis et al. (2017)	CV	Powder	1064 nm	Redder	Darker	X	X	–	–	X	–
Hiroi et al. (2013)	Howardite	Pellet	1064 nm	Redder	Darker						
Hiroi et al. (2013)	Tagish Lake	Pellet	1064 nm	Bluer	Darker						
Kaluna et al. (2017)	Lizardite (Fe-rich)*	Powder	1064 nm	Redder	Darker						
Kaluna et al. (2017)	phyllo.*	Powder	1064 nm	Bluer	Darker						
Prince and Loeffler (2022)	CI-CM simulant	Powder	1064 nm	Redder	Darker						

(CO) undergo a drop in albedo and a reddening of the continuum when exposed to He⁺ ion irradiation, while hydrous meteorite samples Mighei (CM), Alais (CI), and Tagish Lake (C2) show an increase in albedo and bluing when exposed to the same conditions. In a follow-up to this study, Lantz et al. (2018) suggest that space weathering effects depend on petrological type and the initial composition of the meteorite. They conclude that the B-type spectrum of Bennu is most likely a CM-like material that was exposed to weathering. These laboratory results (e.g., Lantz et al. (2017) and Brunetto et al. (2020)) are consistent with ground-based spectroscopic studies of young and old primitive inner-belt families (Campins et al., 2018), which suggests that on Bennu, older terrains should be bluer than younger surfaces. However, complicating this picture, Kaluna et al. (2017) and Gillis-Davis et al. (2017) suggest that spectral reddening is an intermediate step on the way to eventual bluing (a conclusion based on laboratory simulation results using pulsed lasers).

Hapke theory: Theoretical modeling has also been used to contribute to the discussion of space weathering spectral effects. In particular, the methods of Trang and Lucey (2019) have met with success in the case of Earth's moon, and, as we shall see, have also been applied to the case of Bennu (Trang et al., 2021). These models incorporate the theory of Hapke (2001) and the results of Thompson et al. (2019, 2020) and Laczniak et al. (2021) with regards to the experimental formation of submicroscopic opaque production in target materials. Submicroscopic particles are subdivided on the basis of size by Noble et al. (2007) into nanophase (<40 nm) and microphase (>40 nm, <100 μm) particles.

Conflicting results: The conflicting and often inconsistent results from laboratory experiments and telescopic observations paint a complicated picture of space weathering on carbonaceous asteroids. Compared to the Moon and S-type asteroids, carbonaceous asteroids are more mineralogically diverse, which may result in nanoscale space weathering products (e.g., nanoparticles) that are compositionally more variable than their lunar and ordinary chondritic counterparts (Adams and Jones, 1970; Pieters et al., 2000; Gaffey, 2010). In turn, nanoparticle phases produce unpredictable and often competing spectral effects in experimental samples, expanding our understanding of how space weathering processes affect airless surfaces.

By simulating the two major constituent processes of space weathering in isolation from one another, the experiments in Tables 1 and 2 have offered insights into their effects and how to recognize them in returned samples. However, in reality, the two processes occur in tandem with one another, not in isolation, and their effects on asteroid spectra may constructively or destructively interfere.

1.4. Previous sample return of carbonaceous materials

The samples of asteroid (162173) Ryugu returned by the Hayabusa2 spacecraft (Watanabe et al., 2017, 2019) are being analyzed in terrestrial laboratories, and will undoubtedly tell us much about the optical

and microphysical effects of space weathering on dark asteroids. In the first results papers by Yada et al. (2022) and Pilorget et al. (2022) we get a glimpse of the kinds of things we can learn from non-destructive examination of the precious extraterrestrial materials obtained from Ryugu by Hayabusa2 (Clark, 2022). Thus far, the close-up studies of the samples have largely confirmed the remote observations from the spacecraft platform, such as the spectroscopic observations in the near-infrared wavelengths (2.0–3.1 μm) by the Near-Infrared Spectrometer number 3 (NIRS3) (Kitazato et al., 2019).

Artificial impact: The Hayabusa2 mission's impact experiment in April 2019 provided an opportunity to examine the spectral properties of the subsurface and compare it to the surface. For example, Kitazato et al. (2021) investigated the NIRS3 spectra of the small carry-on impactor (SCI) crater region compared with undisturbed regions. The result shows a slightly weaker and peak-shifted OH feature on the surface compared to the subsurface (Kitazato et al., 2021), but no other distinguishing characteristic was observed from the subsurface.

First sample analyses: This result is largely confirmed by the first sample analysis performed by Yada et al. (2022) who find that the returned samples are spectrally very similar to the average surface of Ryugu from 2.0–3.1 μm. The returned samples show a band at 2.7 μm that is 5–10% deeper (and slightly wider) than average Ryugu, and they are brighter at 2.0 μm than average Ryugu by about 0.2–0.25%. These minor differences may be due to space weathering of the average surface, assuming the samples represent the subsurface. However, spectral comparisons are difficult due to differences in spatial and spectral resolution between the remote spacecraft platform and the laboratory spectrometer.

On average, laboratory observations of the soil of Ryugu at the millimeter scale by Pilorget et al. (2022) agree with spacecraft-based remote observations at the meter scale. In fact, for the most part, the samples seem to be representative of the surface of Ryugu, even though they were obtained from two distinct locations, and even though the sampling events may have collected material from different depths of the subsurface.

Suggested analog: Yada et al. (2022) find evidence in favor of CI chondrites as the best analog for Ryugu surface materials, but emphasize that the Ryugu samples are darker, more porous, and more fragile than CIs.

1.5. Previous work on the timescales of space weathering

In the recent past, our understanding of asteroidal surface evolution and space weathering rates has relied upon spectroscopic studies to determine the timescales involved in such processes (e.g. Jedicke et al. (2004) and Vernazza et al. (2009)). Specifically helpful are the reflected light spectroscopy investigations of time-dependent alteration of ordinary chondrite meteorite reflectance spectra (Sasaki et al., 2001).

This alteration makes ordinary chondrite meteorite reflectance spectra resemble the overall spectral shape and slope of S-type asteroid spectra (Clark et al., 2002; Gaffey, 2010).

Asteroid families: One fruitful approach to the study of space weathering rates has been to determine ages of asteroid families by dynamical modeling and consider the spectral properties of the daughter fragments (e.g., Vernazza et al. (2009), Marchi et al. (2012) and Willman et al. (2010)). For example, Vernazza et al. (2009) concluded that solar wind interactions dominate asteroid space weathering on timescales of $10^4 - 10^6$ years. Indeed, there is some overlap between inferred space weathering timescales derived from analysis of asteroid family spectra and models of the two primary space weathering processes (e.g. Jedicke et al. (2004), Nesvornỳ et al. (2005), Christoffersen and Keller (2015), Marchi et al. (2012) and Shestopalov et al. (2013)). Space weathering rate estimates based on modeling vary from $10^4 - 10^6$ years for solar wind irradiation (Hapke, 2001; Loeffler et al., 2009) to $\sim 10^8$ years (Sasaki et al., 2001) for impact processing on typical S-type asteroid materials. Shestopalov et al. (2013) suggested that impact gardening of regolith particles and asteroid resurfacing counteract the rapid progress of solar wind optical maturation and proposed a characteristic space weathering timescale of $\sim 10^5 - 10^6$ years. Similar experiments have been performed on C-complex asteroid analog material with appropriate energies and fluxes, giving equivalent timescales (e.g. Lantz et al. (2015, 2017)).

Samples from S-Types: The most direct constraint on asteroidal space weathering rates thus far comes from studies of the regolith particles from the S-type asteroid Itokawa returned by JAXA's Hayabusa mission. The Itokawa particles have rims formed by a combination of solar wind irradiation and vapor deposition (e.g. Noguchi et al. (2014)). Many of the particles contain solar flare energetic particle tracks, and the track density can be used to infer exposure ages and regolith dynamics on the parent body (Keller and Berger, 2014; Noguchi et al., 2014). The highest solar flare track density observed to date is 5×10^9 cm^{-2} in a plagioclase grain, corresponding to a space exposure age of $\sim 110,000$ years (Keller and Berger, 2017). Provided the track measurements are typical for Itokawa surface particles, these results suggest that the space weathering rate to convert ordinary chondrite materials to resemble S-type asteroid spectra (e.g. Bonal et al. (2015)) is on the order of $\sim 10^5$ years.

2. Evidence from OSIRIS-REx

2.1. Imaging observations

Imaging data are useful for studying crater size frequencies and other time-dependent phenomena on the surface of Bennu, but they are also useful for study of color contrasts that might be due to surface evolution. The MapCam and PolyCam imagers of OSIRIS-REx Camera Suite (OCAMS) (Rizk et al., 2018) returned multispectral medium angle and panchromatic narrow angle images, respectively, of Bennu during OSIRIS-REx proximity operations (Lauretta et al. (2022), DellaGiustina et al. (2019, 2020)). MapCam obtained images in four narrowband $(60 - 90$ nm wide) color filters, referred to by their designation: b', v, w, and x, with center wavelengths at approximately 473 nm, 550 nm, 698 nm, and 847 nm, respectively (Golish et al., 2020). MapCam and PolyCam also acquired panchromatic data with a broad filter (~ 300 nm wide centered at 646 nm) (Bennett et al., 2021; Burke et al., 2021).

Small red craters: Bennu has a global average geometric albedo of $4.4 \pm 0.2\%$ (Golish et al., 2021), consistent with a high carbon or organic material content, and has been shown to be most closely related to CI and/or CM carbonaceous meteorites (Clark et al., 2011; Hamilton et al., 2019; Simon et al., 2020a) or even CR meteorites (Hamilton et al., 2022). Bennu's global average moderately blue color (or spectral slope) was originally detected in telescopic data (Clark et al., 2011) and then confirmed by the spacecraft encounter in both imaging and spectral data (DellaGiustina et al., 2019; Simon et al., 2020a; DellaGiustina et al., 2020). Against this background, DellaGiustina et al. (2020) found a number of small, darker, and spectrally redder (at visible wavelengths) craters (Fig. 1) in MapCam observations. (Note that even the reddest small craters on Bennu are spectrally blue. Thus, when we say redder in the context of Bennu, we mean less blue, relative to the average.)

These small features are abundant, and their size-frequency distribution led DellaGiustina et al. to suggest that they are the youngest craters on Bennnu. Likewise, the poleward faces of large boulders on Bennu tend to be redder (at visible wavelengths) than their equatorial faces, indicating that solar exposure and micrometeoroid impacts cause spectral bluing over time. Craters formed within individual boulders (Ballouz et al., 2020) also appear redder (at visible wavelengths) than their surroundings (DellaGiustina et al., 2020). On the basis of crater and boulder colors, DellaGiustina et al. conclude that, with age, surface materials eventually brighten across all visible wavelengths and become more neutrally sloped, consistent with Bennu's gently blue average visible spectrum. Crater superposition relationships indicate that the timescale of these color changes is $\sim 10^5$ years. In sum, DellaGiustina et al. attribute the reflectance and color variations currently present in Bennu color imagery to a combination of primordial mineralogical heterogeneity and varying exposure ages.

Textural diversity: Images of Bennu obtained at higher spatial resolution with PolyCam revealed a rough, rocky surface covered with boulders (ranging in size from decimeters to 95 meters in diameter) that show a wide range of textural diversity (DellaGiustina et al., 2019; Rozitis et al., 2020). DellaGiustina et al. (2020) describe two main boulder populations: relatively bright boulders that are >4.9% in normal albedo, and dark boulders that are ≤4.9% in normal albedo. (In this context, "normal" means that the surface is illuminated and observed at zero degrees incidence, emission, and phase angle (e.g., see Li et al. (2015) for a full description of normal albedo). The dark boulders appear to have much rougher and more textured (like cauliflower) surfaces than the bright boulders Walsh et al., 2019; Rozitis et al., 2020; DellaGiustina et al., 2019). These observations raise the question of whether the texture variations on Bennu are causing the color and albedo variations, or whether they are related to different boulder compositions (e.g. Rozitis et al. (2022)) and/or optical modification by space weathering.

Effects of texture: In a laboratory study of a mixture of phyllosilicates and carbon lampblack – an approximate analog for Bennu (Cloutis et al., 2011, 2018) – Sen et al. (2021b) showed that strong color and albedo changes can occur as a result of texture variations, independent of compositional changes or surface maturation. For example, in the laboratory, a 36% brightening occurs (at visible wavelengths) when texture changes from rough broken rock to sanded slab (at 550 nm), and a 13% brightening occurs when coarse particles are reduced to fine powders. In association with these albedo changes, Sen et al. (2021b) describe a 14% bluing (in 473 nm/847 nm color ratio) when the texture changes from rough broken surface to sanded slab, and 18% reddening when coarse particles change to fine powder. Previous workers have also found that particle size has strong effects on spectra (Johnson and Fanale, 1973; Beck et al., 2010; and others.) Boulders on Bennu vary strongly in terms of roughness at the tens of centimeters scale, and probably also at finer scale sizes (DellaGiustina et al., 2019). Thus, some of the imaging color variations on Bennu may be consistent with texture changes and/or with surface maturation. With a small twist on this theme, it is conceivable that surface maturation is coincident with texture changes. Indeed, DellaGiustina et al. (2020) highlight that small red craters on Bennu also appear to have a higher proportion of fine grains and appear texturally distinct from their surrounding terrain (Fig. 1).

Resurfacing: Morphologic features across the surface of Bennu also show that Bennu has an active resurfacing process in the form of mechanical breakdown (Fig. 2). This is documented in Molaro et al.
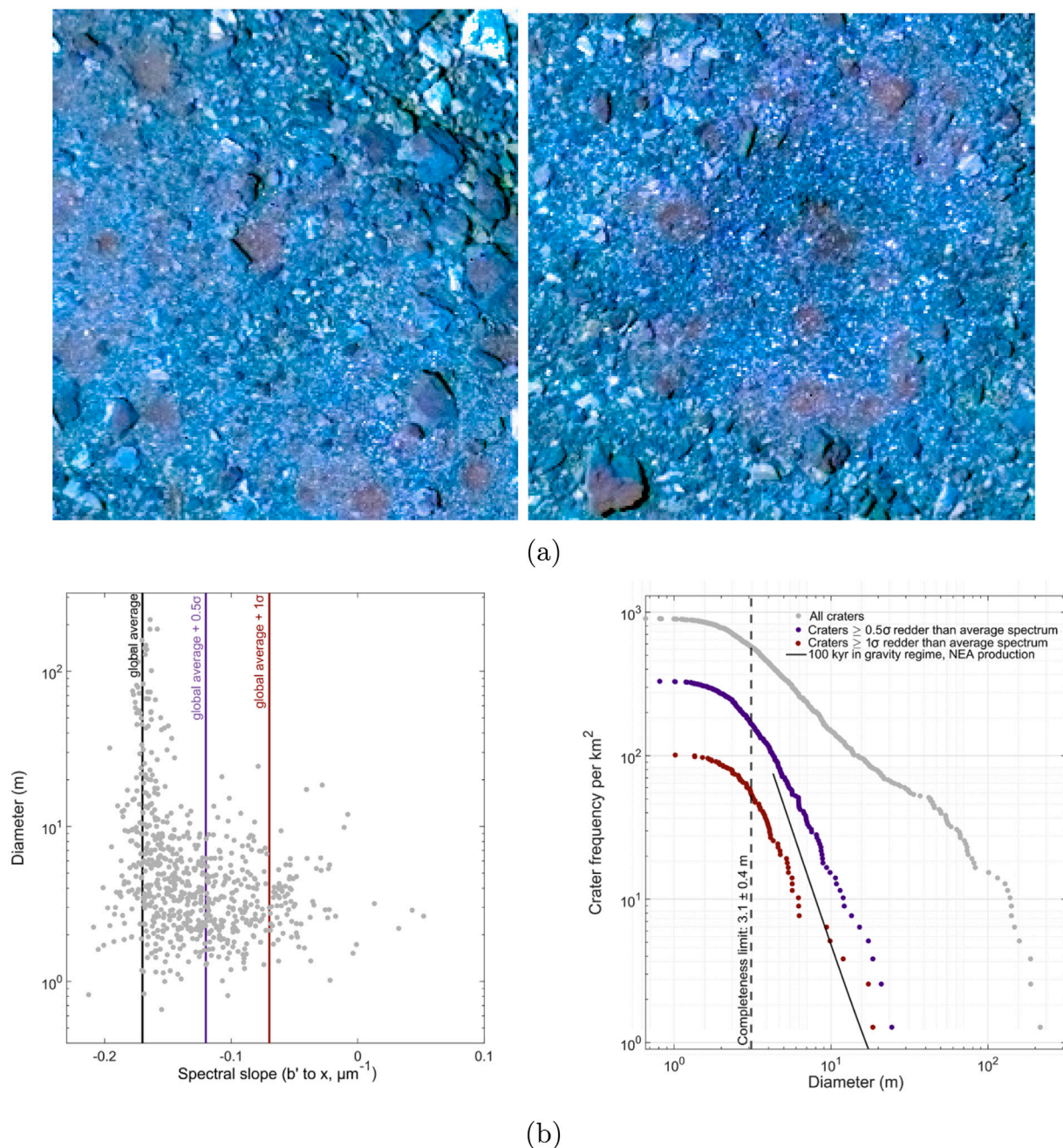
Fig. 1. (a) shows examples of the small red-colored craters found on Bennu, and (b) shows statistical distributions of crater diameters. The red circular depressions are all craters less than 10 m in diameter (top left). The right frame encloses an older crater that is superimposed by the younger red craters. This shows that over time, crater colors eventually blend into the average blue-ish color of Bennu's global materials. (For interpretation of the references to color in this figure legend, the reader is referred to the web version of this article.)
Source: Adapted from DellaGiustina et al. (2020).

(2020a) and Delbo et al. (2022) in terms of statistics of the occurrence of thermal cracks and exfoliation, illustrated with maps of the locations and orientations of features found to date. Indeed, Cambioni et al. (2021) report an inverse correlation between the abundance of fine particles (smaller than a centimeter in diameter) and the porosity of rocks on Bennu. They interpret this to mean that fine particle accumulation is prevented by highly porous rocks and boulders. In addition, the many particle ejection events observed in images captured by OSIRIS-REx navigation cameras, described in Lauretta et al. (2019) and Hergenrother et al. (2020), also indicate the action of a surface refreshing process that may be related to the mechanical breakdown described in Molaro et al. (2020a,b). To date, it has not been possible to

link a particle ejection event to a color or albedo change at the surface of the asteroid. However, it is clear that currently active processes are supplying fresh (unweathered and immature) materials to the surface of Bennu.

Mass movement: In a study of the geopotential on Bennu, Scheeres et al. (2019) found that the terrain slope distribution is consistent with a model of regolith failure and mass movement on rapidly spinning spheroidal bodies detailed in Scheeres (2015). As a body's rotation accelerates (perhaps due to Yarkovsky–O'Keefe–Radzievskii–Paddack (YORP) thermal radiation forces), the slopes tend to increase until failure occurs, which triggers mass movement toward the global geopotential low. Newly exposed material would be left behind and would
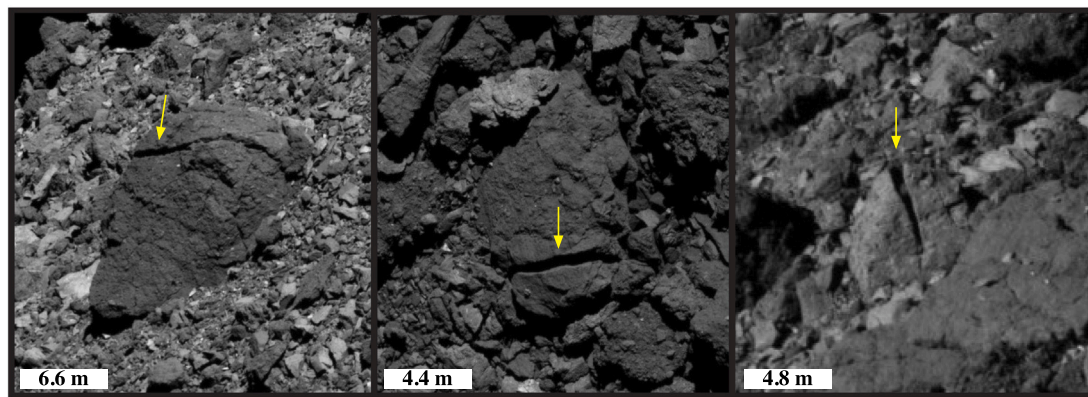
Fig. 2. This figure shows examples of cracking and mechanical breakdown of boulders found on Bennu as a result of thermal processes. (For interpretation of the references to color in this figure legend, the reader is referred to the web version of this article.)
Source: Adapted from Molaro et al. (2020a).

tend to have the angle of repose. The latitudes and manner in which failure occurs depend on the spin rate and regolith friction angle. Signs of mass movement on Bennu, identified by Jawin et al. (2020), include boulder burial, rocks perched on other rocks, particle size grading, axis alignment, imbrication, and even a single large mass flow. The direction of mass movement is strongly correlated with the present-day local downslope direction, which on Bennu is ubiquitously directed toward the equator, the global geopotential low (Scheeres et al., 2019).

Sampling event: During sample collection in October of 2020, the OSIRIS-REx spacecraft excavated a $9 \, m \times 6.5 \, m$ crater on the surface of Bennu, revealing the asteroid's subsurface material (Lauretta et al., 2022). A cloud of dust was quickly produced by the disturbance of the surface by the sampling operation—and lofted upwards towards the spacecraft. Comparisons of imaging data from before and after sampling show that the freshly exposed subsurface material in the crater is darker and redder than the pre-disturbannce surface. This is taken as evidence that fresh surfaces exposed by cratering on Bennu mature over time from redder and darker to brighter and bluer (Lauretta et al., 2022), supporting the proposal of Lantz et al. (2018) and DellaGiustina et al. (2020). However, it is also possible that the observed differences could be caused by textural changes created by the impact. The cloud of dust lofted by the impact is composed of fine particles that eventually settle out close to the impact site, and smaller particles are spectrally redder than coarse particles, consistent with the observations. However, smaller particles are also usually brighter than coarse particles (Johnson and Fanale, 1973), which is not observed.

2.2. Spectroscopy observations

2.2.1. Visible to near-infrared observations

Spectroscopic evidence about space weathering on Bennu was obtained in the visible to near-infrared wavelengths (0.4 to 3.7 μm) by the OSIRIS-REx Visible and InfraRed Spectrometer (OVIRS) (Reuter et al., 2018; Simon et al., 2018). The global OVIRS survey data of Bennu are photometrically modeled and corrected for variations in local incidence and emission angles in Zou et al. (2021). On average, Bennu's global OVIRS spectrum is characterized by a smooth, relatively featureless, spectrally blue-sloped continuum accented by a strong hydration absorption feature at 2.7 μm that is observed ubiquitously across the surface of Bennu (Hamilton et al., 2019; Simon et al., 2020a). Spatially resolved data (as opposed to whole-disk spectra obtained on approach) also show an absorption feature indicative of organics and carbonates near 3.4 μm (Simon et al., 2020a). This feature is stronger in spectra obtained when the spacecraft was closer to the surface. It is analyzed and mapped in detail in papers by Kaplan et al. (2020), Ferrone et al. (2021) and Kaplan et al. (2021). In particular, Ferrone et al. show that the feature is consistent with carbonates in 69% of all detections at the

spatial scale of 4–9 m/spectrum, and consistent with organics in 31% of cases. Furthermore, they find that the organics are more concentrated near the OSIRIS-REx sampling site than the carbonates, suggesting that the returned samples may prove to be organic-rich.

Crater spectra: Deshapriya et al. (2021) conducted a study of the subtle but systematic variations in spectra of craters on Bennu. They found a shortward shift of up to 25 nm in the minimum position of the 2.7 μm band minimum (that may be consistent with reddening, but is not accompanied by a decrease in band depth) relative to the global 2.7 μm band minimum, for 20 out of 45 craters. They attribute this shift to the presence of relatively fresh (less space-weathered) material excavated from the sub-surface by crater-forming impacts. In several cases, Deshapriya et al. (2021) observed that spectra become redder and darker towards the center of the crater, and they attribute this to the presence of fine-particulate regolith. In addition, assuming that craters on Bennu's equator are the oldest geological features on the surface, they find that younger craters are redder and brighter in the OVIRS wavelengths and have deeper 2.7 μm bands than older craters. (But interestingly, they find that the crater hosting the OSIRIS-REx sample site, Nightingale, is both the reddest and the darkest, complicating this relationship.) Taken altogether, these trends suggest that young craters on Bennu reveal fresh subsurface material that is brighter in the OVIRS wavelengths and more hydrated than its surroundings; it is also spectrally redder because it is in the form of fine grains. According to Deshapriya et al. (2021), these crater materials evolve over time (get darker and bluer in the OVIRS wavelengths) to assume the global average spectral properties of Bennu, such that older craters are indistinguishable from average Bennu.

The hydration feature: Praet et al. (2021) performed a detailed analysis of the 2.7 μm band, using an approach developed by Milliken and Mustard (2007) where the effective single-particle absorption thickness (ESPAT) of a spectrum can be linked directly to water content (see also Milliken and Mustard (2005) and Garenne et al. (2016)). Among their results, Praet et al. find that H abundance has a latitudinal dependence: equatorial latitudes show a 9% decrease in H content as compared to average Bennu. They demonstrate that Bennu's strong 2.7 μm hydration band is shallower around the equator, and they attribute this decrease in band depth to partial dehydration of the surface (Fig. 3).

Spectral modeling: In their study using Hapke modeling to fit the visible wavelength spectra of Bennu, Trang et al. (2021) incorporated the optical effects of nanophase and microphase metallic iron, troilite, and magnetite, because they are all observed byproducts that form in laboratory simulations of space weathering of various substrates (Thompson et al., 2019, 2020). Nanophase iron, in particular, is an important component of strongly space-weathered soils from the Moon (Cassidy and Hapke, 1975; Hapke, 2001). Trang et al. suggest that
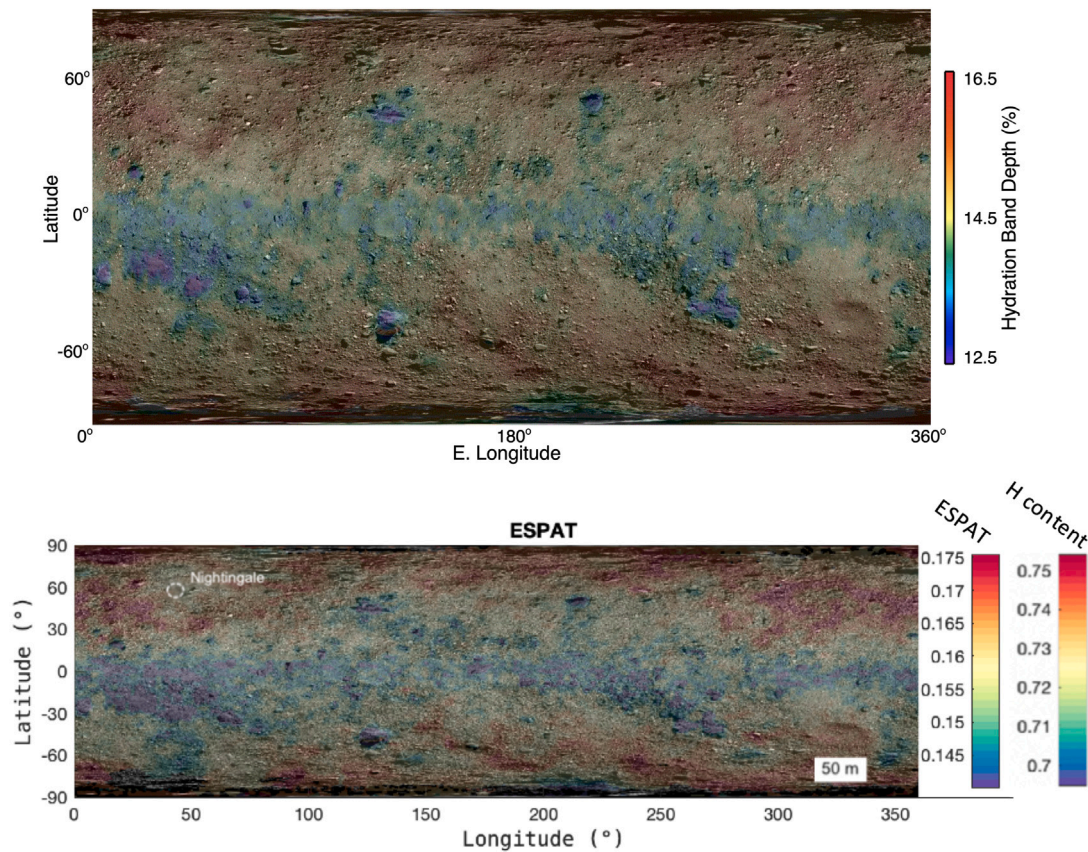
Fig. 3. The top panel shows a 2.7 μm band depth map from OVIRS measurements, reproduced from Simon et al. (2020a). The bottom panel shows an ESPAT map of Bennu at 2.7 μm adapted from Praet et al. (2021): spectral data at 20 m/footprint are converted to ESPAT and corresponding H content. This projection shows longitudes from 0° to 360° longitude. Both maps are overlain on the global image-mosaic basemap of Bennu (Bennett et al., 2021). (For interpretation of the references to color in this figure legend, the reader is referred to the web version of this article.)

on Bennu, space weathering results in nanophase magnetite forming first, followed later by nanophase iron. They conclude from their mapping efforts that magnetite is more abundant than metallic iron on Bennu, causing the overall blue color, and they suggest that nanophase and microphase troilite may also be present (Trang et al., 2021). This idea is corroborated by observational evidence for magnetite presented in Lauretta and DellaGiustina et al. (2019), Hamilton et al. (2019), and Simon et al. (2020b). The Trang et al. (2021) study nicely accounts for the color differences associated with the different nano/microparticles, and explores the role of hydration in determining which nano/microparticles form first during space weathering. We note, however, that it is easy to simulate the global average blue spectral behavior of Bennu in the lab without space weathering products; just by using other important compositional components of the Bennu spectrum: phyllosilicate (in the form of saponite) and carbon (in the form of lampblack powder) (Sen et al., 2021b) or magnetite, also in the form of powder (Cloutis et al., 2011). In addition, Merlin et al. (2021) have shown that Bennu can be accurately modeled using Hapke theory and various mixtures of spectra of meteorites from the existing collection: heated CM, C2-ungrouped, and CI meteorites.

Photometric studies: Spectrophotometric analysis of OVIRS data (Li et al., 2021) shows that, on a global scale, the equatorial region of Bennu exhibits properties that are distinct from other regions, and both a latitudinal trend and a slight north-south asymmetry exist (Fornasier et al., 2020; Li et al., 2021). In the near-infrared wavelengths from 0.5–2.5 μm, the equatorial region appears to be redder than the mid- to high-latitude regions (consistent with ground-based telescopic measurements by Binzel et al. (2015)), and the spectral slope decreases towards higher latitudes (Fig. 4). The spectral reddening of the equatorial band is consistent with findings from other analyses

(Simon et al., 2020a; Barucci et al., 2020). In addition, the equatorial region also shows a weaker phase reddening than the global average, although the difference is subtle. Also, a slight asymmetry exists, where the southern hemisphere may be slightly rougher at the μm-scale, and shows a slightly weaker phase reddening than the northern hemisphere. This result could be correlated with the findings of Daly et al. (2020) who used the OSIRIS-REx Laser Altimeter observations to create a global shape model of Bennu with 20 cm resolution. They conclude that Bennu's southern hemisphere is rounder and smoother at the >20 cm scale because it has more numerous large boulders that retain surface materials and provide more strength at depth to support them, whereas Bennu's northern hemisphere has higher slopes and a less regular shape because it has fewer large boulders and more evidence of boulder downslope movement.

The spectral color and phase reddening of the equator do not appear to be correlated with the albedo patterns on Bennu on the global scale (see Simon et al. (2020a)). Rather, the albedo patterns appear to be correlated with the morphologies and textures of boulders (DellaGiustina et al., 2020). Li et al. (2021) attributed the equatorial banding and latitudinal trends found in the OVIRS spectrophotometry of Bennu to latitudinal mass movement (Jawin et al., 2020) caused by the distinct geophysical conditions on Bennu (Scheeres et al., 2019, 2020). If this is correct, then the latitudinal spectrophotometric trends (darkening and reddening along the equator) are likely to be associated with processes that alter the optical and mechanical properties of Bennu's surface material, including space weathering, rather than associated with composition. The largest dark boulders are all at high latitudes (DellaGiustina et al., 2020) and the brighter boulders are predicted to be mechanically stronger and may survive migration to the equator better than the dark, weaker boulders (Rozitis et al., 2020). Thus, mass

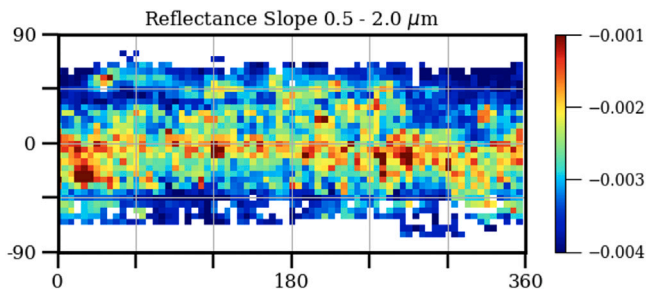**Fig. 4.** This figures shows a spectral reflectance slope map of Bennu from OVIRS measurements from 0.55 μm to 2.0 μm, binned in 1° × 1° squares (each grid element is ~4.3 m wide at the equator).
Source: Adapted from Li et al. (2021).

movement on Bennu could be acting to sort the various levels of surface alteration along the latitudinal direction, thus affecting the micro-scale texture and structure of regolith particles, resulting in the observed spectrophotometric effects.

Latitudinal trends: To investigate the latitudinal trends that are hinted at in the Li et al. (2021) study, Sen et al. (2021a) tested whether the latitude dependence of spectral properties on Bennu is statistically significant. They calculated average spectral parameters as a function of latitude in 2° bins using both a regionally photometrically corrected data set (Li et al., 2021) and a global photometric model data set (Fig. 5) (Zou et al., 2021). Fig. 6 shows latitudinally averaged values for several spectral parameters of interest using these data sets: albedo (normal reflectance at 0.55 μm) (Fig. 6(a)), spectral slope from 0.5–1.5 μm (Fig. 6(b)), band depth at 2.74 μm (Fig. 6(c)), and depths of the minor bands identified by Simon et al. (2020b) at 0.55 μm, 1.05 μm, and 1.81 μm (Fig. 6(d)). While Sen et al. (2021a) find only a very weak latitude dependence signal in the minor bands of Simon et al. (2020b) Fig. 6(d) (right), the other figures show a signal of latitude dependence with at least 2-sigma statistical significance that is especially strong in the spectral slope and hydration band depth spectral parameters (Figs. 6(b) and 6(c)). This latitude dependence is consistent with processes that are heliocentric in nature, such as solar wind irradiation, and micrometeoroid bombardment, both of which are implicated in space weathering processes (Hemingway et al., 2015). While other physical changes, such as porosity and particle size can also cause such spectral trends, it is difficult to explain why they would be latitude-dependent. However, porosity, particle size, and even temperature of materials cannot be ruled out as potential causes because regolith-gardening by impact may also be latitude-dependent: Gallant et al. (2009) find a latitude dependence in the impactor populations at the Earth and Moon indicating impact shadows at the poles of each object, and Bottke et al. (2020) also suggest a latitude dependence in impactor flux on Bennu. We suggest space weathering as the most likely explanation because crater counting evidence indicates that the equatorial surface is the oldest surface on Bennu (Bierhaus et al., 2022), making large-scale turnover of the regolith by large impacts unlikely.

Fig. 6(a) (right) shows a peak in albedo along the equator, while 6(a) (left) shows a peak in albedo at +35° latitude. It is possible that the Fig. 6(a) (right) panel is showing that our observation methods are biased by the fact that the OVIRS data of Bennu that have low incidence and emission angles were obtained along the equator, causing the global average model to indicate that the equator is brighter, when in fact it is not. However, the regionally calculated photometric model by Li et al. (2021) can partially account and correct for the observational bias (Fig. 6(a) (left)). We also see a considerable increase in spectral slope at the equator in this model (Fig. 6(b)), which could be explained by a particle-size effect. As shown by Sen et al. (2021b), particle size-effect continuum slope reddening, due to finer particles, is usually accompanied by an increase in albedo.

Artificial crater: OVIRS observations of the artificial crater created on Bennu by the OSIRIS-REx sampling event, analyzed in Lauretta et al. (2022), indicate that fresher materials (very recently excavated by the sampling event) are darker and spectrally redder than their surroundings and than the pre-sampling surface at that location. Images from the sampling event indicate that a cloud of fine particles was created, and the sampling site was finer-grained after the sampling event. From Sen et al. (2021b), we know that a decrease in particle size and a refinement of texture (between 'very rough' rock and 'smoother' sanded slab) both cause reddening and brightening. Post-sampling event colors could thus be explained by finer particles or smoother surfaces, but the accompanying drop in albedo indicates coarser particles or rougher surfaces, and hence inconsistent results. Thus, texture change is not the preferred explanation of the pre-sampling vs. post-sampling color/albedo comparisons. Rather, the likely explanation is that the excavation of the crater exposed finer, redder, darker material in the subsurface, consistent with the space weathering models of Lantz et al. (2018) and DellaGiustina et al. (2020).

2.2.2. Thermal infrared observations

Thermal infrared radiation measurements can inform space weathering studies by providing emissivity spectra and information about surface conditions, such as thermal inertia, roughness, grain size, porosity, and dust coating. Because all these factors can alter visible, near-infrared, and thermal infrared radiation, consideration of each factor is necessary for interpretation of remotely sensed information.

Instruments and measurements: On Bennu, thermal and short-wave infrared radiation were measured with two instruments: the OSIRIS-REx Thermal Emission Spectrometer (OTES) (Christensen et al., 2018) and OVIRS (Reuter et al., 2018). While OTES is designed to measure thermal emission, OVIRS serendipitously obtains a measure of it at the short wavelength end of the blackbody curve, also known as the "thermal tail", because Bennu is so warm. These instruments obtained global measurements at seven different times of day, as reported in Rozitis et al. (2020) and Zou et al. (2021). During approach of the OSIRIS-REx spacecraft, measurements of the sunlit thermal radiance of Bennu indicated surface temperatures ranging from 200 K to 350 K (−100° to 170 °F) (DellaGiustina et al., 2019; Rozitis et al., 2020).

Thermal inertia: Rozitis et al. (2020) calculated a thermal conductivity for the boulders on Bennu that is lower than any measured meteorite thermal conductivity value. However, among Bennu's two primary populations of boulders (dark and brighter), the brighter boulders (thermal inertia unit (tiu) values of 400 to 700) may have thermal inertias that, according to Rozitis et al. (2020), approach CM chondrite values. Thus, CM and similar meteorites may be similar to the brighter boulders in density and porosity, whereas the dark boulders have thermal conductivities and thermal inertias (tiu values of 180 to 250) far below those of the meteorite collection and likely are distinct from any recognized meteorite types in terms of their thermomechanical properties.

Surface roughness: Rozitis et al. (2020) find mean surface roughness values from OTES and OVIRS to be (40 ± 2)° and (40 ± 3)° RMS slope, respectively. Variations in thermal roughness across the surface largely coincide with variations in the surface concentration of boulders visible in imaging.

Dust cover: Hamilton et al. (2021) reported that the OTES observations of Bennu are most consistent with laboratory measurements of solid substrates with very thin accumulations (a few to tens of microns, or just a single layer) of fine particles (<~65 −100 μm). The dustier surfaces commonly correspond to rougher rocks that may produce and/or act as traps for the particles, but the dust may also accumulate in cracks and depressions throughout the surface. In addition, sample collection from the surface of Bennu using gas stimulation mobilized a reservoir of fine, sub-mm dust particles (Lauretta et al., 2022). Disaggregated boulder particles may have contributed to this cloud, however (Lauretta
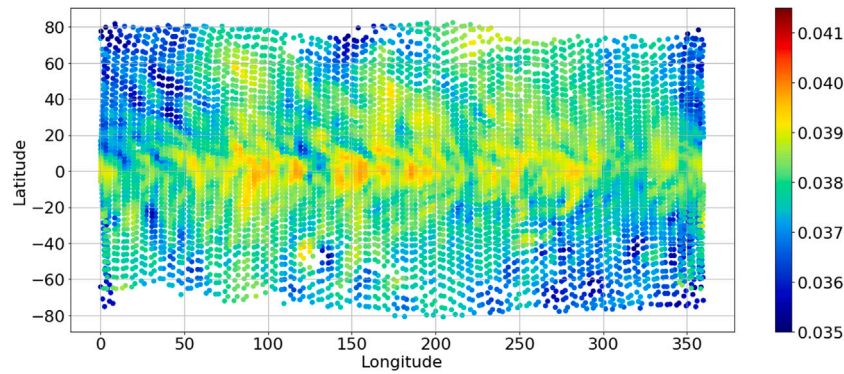
Fig. 5. Global photometric model RADF at 0.550 μm from OVIRS calculated for the Bennu v20 stereophotoclinometric shape model (Barnouin et al., 2019) as observed during OSIRIS-REx's 12:30pm Equatorial Station observation of Bennu (also known as EQ3), using the McEwen photometric model function (Zou et al., 2021).

et al., 2022) concluded that some of the cloud consisted of existing dust liberated from the surface or near-subsurface.

Porosity: In the summary by Rozitis et al. (2020), models for thermal conductivity as a function of porosity predict that the darker boulder thermal inertia of $180-250$ tiu would correspond to a porosity value of $49-55\%$, whereas the brighter boulder thermal inertia value of $400-700$ tiu corresponds to a porosity of $\sim24-38\%$, at least within the upper few centimeters of the exposed surface.

Emissivity spectra: Laboratory measurements by Lantz et al. (2017) highlight a systematic shift (of about 0.1 μm) of the phyllosilicate bands at 2.7 μm and 10 μm toward longer wavelength, independent of the initial composition of the sample (more or less hydrated, more or less rich in C content). Further analysis showed that bands in the thermal infrared shift the same way for all samples and that their relative intensities differ after irradiation (Brunetto et al., 2020). If the lab simulations are representative of what happens on natural surfaces, the band shift should be detectable on Bennu by OTES. In particular, chances are good for detecting this effect in the 10 μm band, where the OTES spectral sampling is very high ~9 cm^{-1} and we are looking for spectral shifts of a few tens of cm^{-1}.

Variability in OTES data was identified during the global mapping phase. Two spectral types have been defined according to the position of the silicate stretching minimum (typically occurring in the 8–12 μm range); OTES Type 1 spectra exhibit a minimum near 987 cm^{-1} and Type 2 spectra have a minimum near 814 cm^{-1} (Hamilton et al., 2021). These differences are primarily attributable to particle size variations based on the paucity of Type 2 spectra in the nighttime data (when the lowest thermal inertia materials contribute the least to the measured spectrum). A study searching for space weathering on Bennu using spectral indices in the mid-infrared wavelength range found a third population (Type 3) with a minimum located near 920 cm^{-1} in the daytime data (Lantz et al., 2020). If we assume that the Type 1 spectra represent a relatively young surface, then areas with Type 3 spectra where the band position is comparable to the shift measured on irradiated CCs may represent space-weathered surfaces. However, more analysis is needed to confirm this result.

In addition, Brunetto et al. (2020) show a match between the OTES global average spectrum of Bennu and an irradiated mixture of the C2 chondrite Tagish Lake and the CM chondrite Mighei (Fig. 7). This spectroscopic match indicates that, on average, Bennu's surface is consistent with solar wind maturation of subsurface C2/CM-like materials. An alternative explanation is that Bennu is not yet very weathered, but has a composition that mimics this irradiated mixture of CC materials (which seems unlikely).

Rozitis et al. (2020) found that Bennu's thermal inertia is in the same range ((350 ± 20) tiu) but that regolith has higher thermal inertia than boulders (DellaGiustina et al., 2019; Rozitis et al., 2020). The thermal inertia contrasts between regolith and boulders on both asteroids is counterintuitive because regolith, which has higher porosity, usually has lower thermal inertia than boulders.

2.3. Laser altimeter observations

Additional insight about Bennu's surface can be gained from the normal albedo (A_n) measured by the OSIRIS-REx Laser Altimeter (OLA) (Daly et al., 2017). OLA is an active-sensing instrument designed primarily for determining global shape and local topography in preparation for sample acquisition. However, OLA also records the return intensity of its pulses, from which we derived A_n, the surface reflectance at zero phase angle, at 1064 nm wavelength (Neumann et al., 2020).

Normal albedo: The laser returns provide measurements of A_n with globally uniform geometry, as have laser altimeters at other airless bodies (Neumann et al., 2013; Lucey et al., 2014). Such studies demonstrate the utility of laser altimeters to yield global measurements of reflectance free of the confounding effects of illumination and observation geometry. For example, at the Moon, Hemingway et al. (2015) found systematic latitudinal variation in near-infrared spectral properties across the lunar surface, including an increase in A_n with latitude in the 1064 nm Lunar Orbiter Laser Altimeter data. They argue that these trends are caused by a flux-dependent equilibrium between regolith gardening and space weathering agents such as solar–wind-induced alteration of exposed surfaces.

Data processing: The OLA data were collected with the Low Energy Laser Transmitter (LELT) at $\sim600-740$ m range at nearly nadir pointing while Bennu rotated beneath the polar-orbiting spacecraft (Daly et al., 2020). The LELT operated at a 10-kHz firing rate, collecting ~3 billion intensity measurements with ~7 cm-diameter footprints. We only retained data with emission angles $<30°$ from the normal to a triaxial ellipsoid because the intensity measurements degraded in quality rapidly at higher emission angles, due to range-dependent loss in signal-to-noise, and measurement bias due to laser pulse spreading in highly oblique incident geometry. To bring the intensity measurements onto an absolute radiometric scale, we scaled them to have a distribution peak at 0.039 based on the MapCam x-band (849 nm) A_n (Golish et al., 2021) with a correction for the OVIRS 1064 nm/869 nm spectral slope. Here we focus on global trends observed in the OLA A_n measurements and implications for space weathering on Bennu.

Latitude dependence: The OLA data were binned into a map at 16 pixels per degree (~30 cm at the equator) in simple cylindrical projection, which was then smoothed with a Gaussian filter with a full width at half maximum of 60 cm (Fig. 8). The color scale min/max values are set to the 1st and 99th percentiles of the area-normalized A_n distribution computed by grouping the map pixels into $\sim800{,}000$ equal-area bins ~1 m in size. Immediately obvious is a trend of increasing albedo with latitude. The latitudinally averaged profile (Fig. 9, top panel) increases from the minimum of ~0.0368 at the equator to ~0.0409 at 64°N/74°S. This trend represents a substantial fraction of the width of the global area-normalized distribution whose mean and standard deviation are 0.0385 and 0.0025, respectively. However,
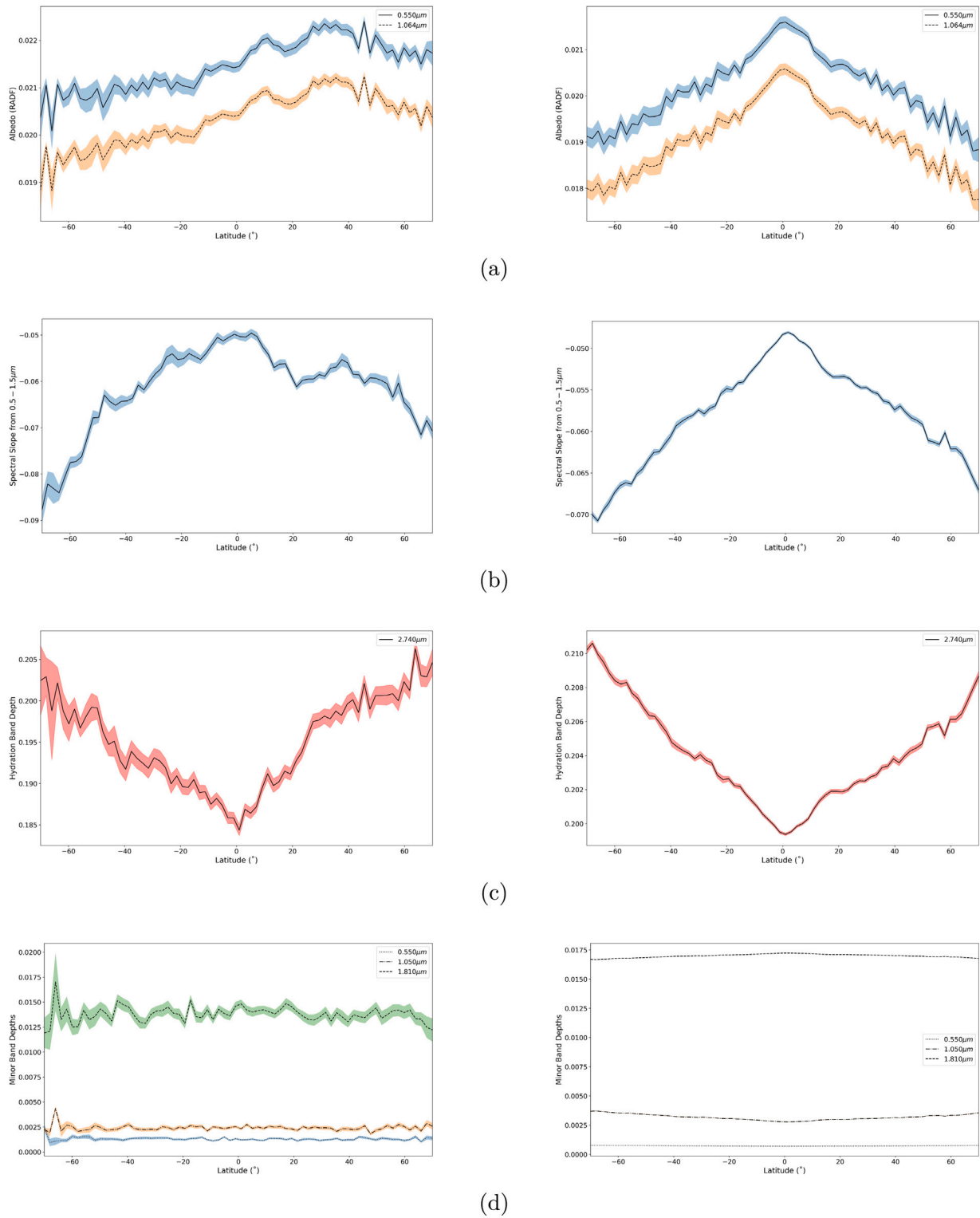
Fig. 6. Bennu (a) albedo, (b) spectral slope, (c) 2.74 μm hydration band depth, and (d) minor band depth averages are calculated for 2° latitudinal bins using regionally photometrically corrected OVIRS data from Li et al. (2021) (left) and photometric model radiance factor calculated using the McEwen model from Zou et al. (2021) (right). In each panel, the shaded area represents standard error of the mean. (For interpretation of the references to color in this figure legend, the reader is referred to the web version of this article.)

subtracting out the latitude trend only reduces the standard deviation by ~12%, highlighting the large albedo variation at any given latitude (Fig. 9, middle panel). The visual perception of a dark band at the equator could be due more to the relative uniformity of A_n within 10° of the equator (Fig. 9, middle panel) than to the mean A_n value itself (Fig. 9, top panel), which continues to decrease toward the equator. The

latitude trends observed at 1064 nm-wavelength also bear similarities to those seen in the distribution of terrain slopes (Fig. 9, bottom panel). The latter has a region of low amplitude terrain slope near the equator, relatively constant higher terrain slope at mid-latitudes, and decreasing terrain slope in the polar regions. The terrain slope distribution and
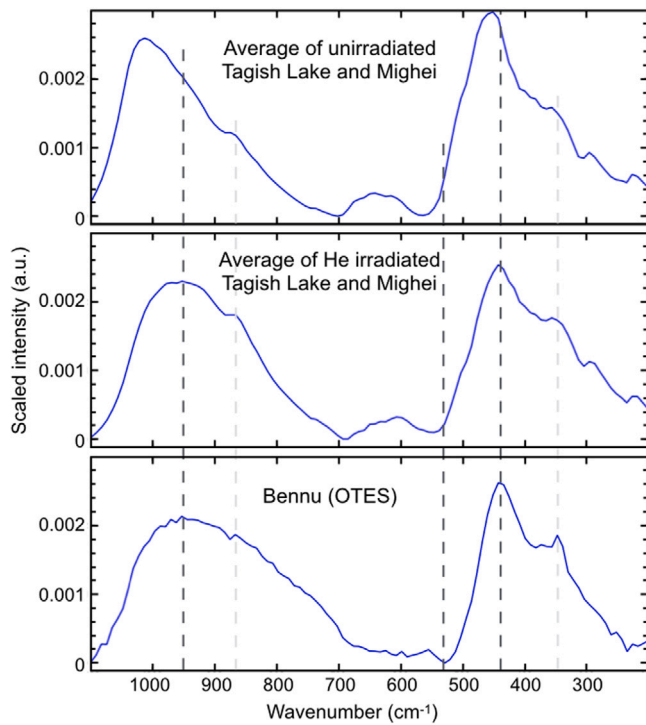
Fig. 7. We see that a linear combination of He-irradiated CM Mighei and C2 Tagish Lake meteorites more closely resembles a hemispherical average of the Bennu spectral data than its unirradiated counterpart.
Source: Reproduced from Brunetto et al. (2020).

the A_n standard deviation are relatively constant within ~10° of the equator.

Considering the above theoretical and observational results especially the result that normal albedo A_n is darker along the equator), it is plausible that material at Bennu's equator has, on average, been exposed to space weathering longer than (or more than) at higher latitudes, which could explain the observed A_n trends if space weathering acts to darken the material at 1064 nm (Sen et al., 2021a; Hemingway et al., 2015).

3. Synthesis

3.1. Previous work and new evidence from OSIRIS-REx

In Table 3 we assemble a list of the observations of Bennu that are relevant to our study of space weathering. While analyses by DellaGiustina et al. (2020) and Rizos et al. (2021) indicate that Bennu brightens and gets bluer with maturation, the Deshapriya et al. (2021) study indicates that Bennu darkens and gets bluer with maturation, consistent with Thompson et al.'s (2020) study of Murchison chip alteration. This discrepancy could be telling us that either the MapCam (DellaGiustina et al., 2020) and the OVIRS (Deshapriya et al., 2021) instruments are sensitive to different surface feature size scales at their different wavelength regimes, or that neither the MapCam nor the OVIRS observations are sensitive to maturation, and both are perhaps seeing the effects of roughness variations at different size scales. While the laboratory simulations of Sen et al. (2021b) support the latter interpretation, they also suggest that if texture contributes to color on Bennu, the texture variations are typically much more subtle than what was simulated in the laboratory. However, the results of Neumann et al. (2020) show a strong latitude dependence of reflectance at 1064 nm with darkening along the equator. Taken together with the results of Li et al. (2021) showing strong latitude dependence of spectral slope

from 0.5 to 1.5 μm (with reddening along the equator), this seems to indicate a pattern of darkening and reddening that is perhaps separate (or operating on a different timescale) from the crater color evolution trends described by DellaGiustina et al. (2020) and Deshapriya et al. (2021).

Particle migration: But the possibility that surface particle movement occurs faster than space weathering maturation must be examined. One possibility that is hard to constrain based on the available literature is that the optical surface of these asteroids may be influenced by a gradual shift in the size of the average grain at the surface over time. In some models, fine grains are lost either to space or by migration downward in the regolith (Ballouz et al., 2019; Miyamoto et al., 2007). Thomas and Robinson (2005), Lauretta et al. (2022) and Walsh et al. (2022) present evidence for very low cohesion in the topmost layers of the regolith on asteroids (433) Eros and Bennu, respectively. Such low cohesion could aid the migration of loosely bound regolith particles to lower geopotential.

Ongoing resurfacing processes are important on Bennu, as shown by Hergenrother et al. (2020), Jawin et al. (2020), Delbo et al. (2022), Bierhaus et al. (2022), and observed color trends are correlated with surface topography, to some extent (Li et al., 2021). Jawin et al. (2020) note that in many locations on Bennu, accumulations of boulders appear to be well sorted: in such places only large meter-scale boulders are visible, without any fine-grained, or unresolved, component. These could be places where surface mass movement has liberated the smaller particles and removed them from the top layer. This process has been suggested for (25 143) Itokawa, where the Muses Sea is composed of well-sorted cm-sized pebbles (Miyamoto et al., 2007), and finer particles are suggested to have been segregated into the interior, or electrostatically levitated and removed by solar radiation pressure (Lee, 1996; Hartzell and Scheeres, 2013), or have had higher impact ejection velocities that restricted their re-accumulation (Nakamura et al., 1994). Thus, on Bennu as on Itokawa, migration of fines may be one of the active surface processes that affects the optical surface – and therefore the colors – of surface features.

Timescales: Based on the distribution of small craters observed on Bennu's boulders, Ballouz et al. (2020) estimate that Bennu reached near-Earth space ~1.75 ± 0.75 Myr ago, which is sufficiently long for the surface to experience the onset of space weathering, according to Vernazza et al. (2009), who estimated that it takes only ~1 Myr for solar wind reddening of S-type asteroids. Based on the distribution of craters >2 m in diameter on Bennu, Bierhaus et al. (2022) suggest that surfaces at the poles and mid-latitudes on Bennu are younger (show more smaller craters) than the equatorial regions (where the largest craters are preserved). These surface crater density differences along with impactor flux estimates allow (Bierhaus et al., 2022) to constrain the oldest surface on Bennu (the equator) to be between 10 and 65 Myr old.

Several other studies provide inferences about timescales involved in surface alteration. For example, Kaplan et al. (2021) describe the composition of the organics found on Bennu by Simon et al. (2020a) and Ferrone et al. (2021), and point out that space weathering could alter organic absorption features, depending on the depth of surface solar wind alteration (Laczniak et al., 2021). So the fact that we see strong organic spectral features may indicate that organic material was recently exposed by impact processes or mass wasting. Extrapolating Bennu's current rotational acceleration back in time, Jawin et al. (2020) inferred that mass movement likely occurred in the past few hundred thousand years at mid-latitude regions on Bennu, where slopes steepened with time by several degrees. In addition, the intriguing discovery that Bennu is an active asteroid with ongoing particle ejections (Lauretta et al., 2019; Hergenrother et al., 2020) leads us to expect the presence of some very young surfaces. Indeed, Delbo et al. (2022) suggest that thermally-induced fractures the length of those on Bennu's boulders can be produced in 10^4–10^5 years. This timescale may be even shorter than processes such as mass movement that expose fresh surfaces, and is very likely shorter than Bennu's lifetime in near-Earth space.
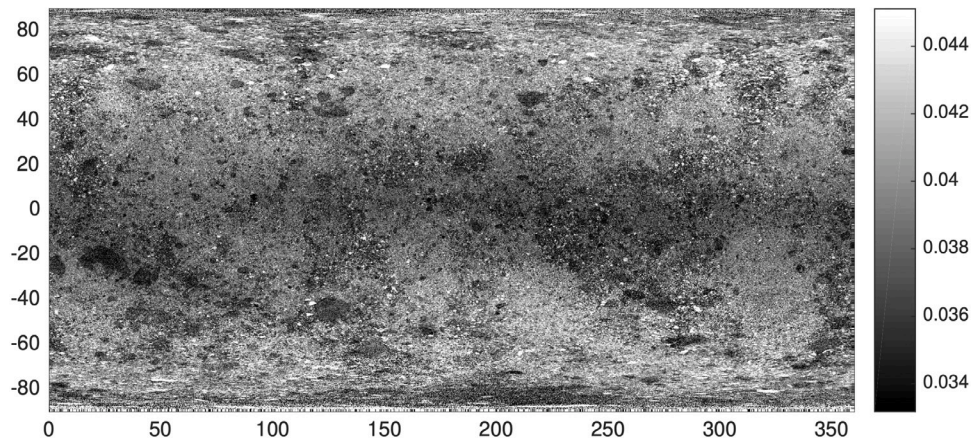
Fig. 8. Normal albedo (A_n) map of Bennu from OLA measurements at 1064 nm, gridded at 16 pixels per degree (~30 cm at the equator).
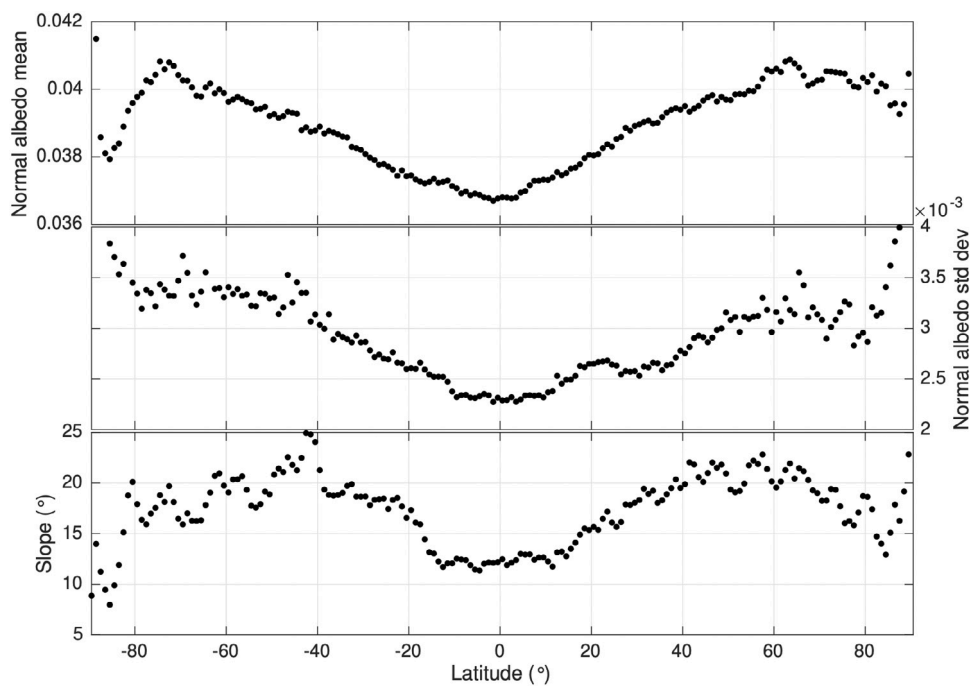

Fig. 9. Latitude trends of normal albedo (A_n) mean (top) and standard deviation (middle), are compared with gravitational slope measured at 3 m scale (bottom). *Source:* Reproduced from Neumann et al. (2020).

3.2. Comparison of Bennu and Ryugu

On Bennu, DellaGiustina et al. (2020) propose that small red craters are likely recently excavated on timescales of 10^5 years, shorter than Bennu's NEA residence time of 1–2.5 Myr as estimated in Ballouz et al. (2020), indicating that Bennu evolved to bluer surface colors in its current orbit. The fact that small craters are distinguishable from the background on Bennu argues that either the rest of the surface is being weathered faster than the global resurfacing rate, or that cratering causes texture changes that fade away over time. Either way, we have an apparent difference between Bennu and Ryugu: on Bennu small (young) craters are red compared with blue surroundings, and on Ryugu small (young) craters are blue compared with red surroundings (Morota et al., 2020).

Divergent color evolution: For this review, we took a closer look at this apparent difference in maturation trends, and find that while the small craters do in fact contrast with their surroundings, the small

reddest craters on Bennu (DellaGiustina et al., 2020) have about the same reflectance spectrum as the small bluest craters of Ryugu (Morota et al., 2020). This is shown in Fig. 10, and is also illustrated more statistically in Fig. 11. This similarity in the colors of the smallest craters on Bennu and Ryugu could mean that fresh materials on the two asteroids have the same starting point in visible wavelength colors before the effects of space weathering begin; however, the subsequent maturation trends move the colors of surface materials in opposite directions in the broadband color parameter space of Fig. 11 (see color arrows). This apparent divergence from the same starting point must be accounted for in any unified model of surface evolution for carbonaceous asteroids.

Hydration feature: It is also interesting to compare the 2.7 μm hydration band shape on Bennu and Ryugu (Fig. 12). Ryugu has a much shallower band (even in the returned samples Pilorget et al., 2022), one that points to less hydrated phyllosilicates, while Bennu's band is quite strong, and points to pervasive aqueous alteration. Thermal effects

Table 3

Here we present a synthesis view of the optical changes that occur with age, as found in various studies of Bennu. In the Albedo column, brighter/darker means relative to surroundings. In the Slope column, redder/bluer means relative to surroundings. (Note that even the reddest features on Bennu are still spectrally blue.) For the artificial crater, which is darker and redder compared with undisturbed surroundings, we tabulate inferred changes with age based on the artificial crater observations, in the same sense as for all other table entries. Also in the Albedo column, units of REFF are Reflectance Factor.

| Literature	Instrument	Location	Albedo	Slope	Band Depth
DellaGiustina et al. (2020)	MapCam	Boulders and craters	7% (0.003 REFF) Brighter at 0.55 μm	43% (0.073 μm^{-1}) Bluer from 0.473 − 0.847 μm	
Deshapriya et al. (2021)	OVIRS	Craters	17% (0.005 REFF) Darker at 0.55 μm	100% (0.3 μm^{-1}) Bluer from 0.55 − 2.0 μm	Younger craters have deeper 2.7 μm band depths, i.e., flattening with age
Lauretta et al. (2022)	MapCam	Artificial crater	3% (0.001 REFF) Brighter at 0.55 μm	87% (10 × 10^{-5} μm^{-1}) Bluer from 0.473 − 0.847 μm)	
Lauretta et al. (2022)	OVIRS	Artificial crater	7% (0.002 REFF) Brighter at 0.55 μm	60% (0.001,5 μm^{-1}) Bluer from 0.5 − 1.0 μm)	2.7 μm band flattening
Li et al. (2021) and Fornasier et al. (2020)	OVIRS	Equatorial band		L: 129% (0.002 REFF) Redder at (0.5 − 2.0 μm); F: 225% (0.045 REFF) Redder at (0.55 − 2.0 μm)	
Neumann et al. (2020) and Daly et al. (2020)	OLA	Equatorial band	11% (0.004 REFF) Darker at 1064 nm		
Simon et al. (2020b,a)	OVIRS	Equatorial band			Flattening of band depths across NIR at equatorial band
Praet et al. (2021)	OVIRS	Equatorial band			2.7 μm band flattening
Sen et al. (2021a)	OVIRS	Equatorial band		Redder at (0.55 − 1.5 μm)	
Hamilton et al. (2021); Lantz et al. (2020) and Brunetto et al. (2020)	OTES	Global			Shift of the silicate NIR (2.7 μm) and MIR (10 μm) bands toward longer wavelengths
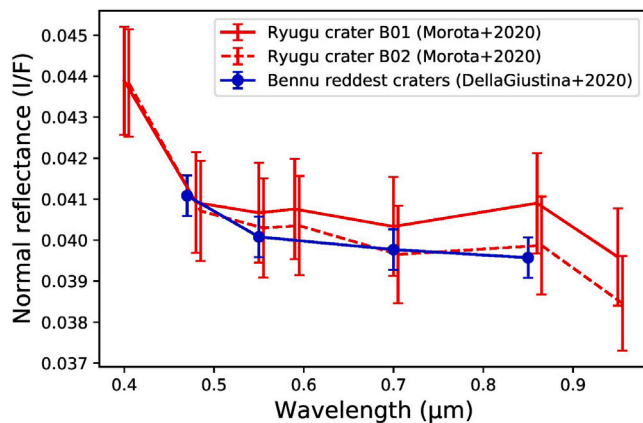
Fig. 10. The bluest small craters on Ryugu (Morota et al., 2020) are compared with the reddest small craters on Bennu (DellaGiustina et al., 2020) in terms of imaging broadband color characteristics. The Ryugu crater colors are from the ONC camera and the Bennu colors are from the MapCam camera. Note that even the 'reddest' small craters on Bennu are spectrally blue. Thus, when we say 'redder' in the context of Bennu, we mean 'less blue', relative to the average. (For interpretation of the references to color in this figure legend, the reader is referred to the web version of this article.)

(such as dehydration) are proposed to explain most of the hydration band spectral changes observed across the surface of Ryugu (Morota et al., 2020; Hiroi et al., 1996). Would such effects also work to explain the hydration band variations on Bennu? Tentatively, we suggest the answer is yes. As shown by Praet et al. (2021), heated CM chondrites and/or Tagish Lake are the best analogs for Bennu based on systematics of the band shape from 2.7–3.0 μm. Praet et al. (2021) used spectra of CM chondrites that were determined to have been naturally heated at some point in their histories, and most heated CMs have experienced temperatures of more than 400 °C (e.g. Lee et al. (2016) and Garenne et al. (2016)). In addition, the hydration band is shallower at the

equator (Simon et al., 2020a), consistent with greater solar insolation expected there.

Takir et al. (2013) show that the shape of the 2.7 μm band in CC meteorites depends on phyllosilicate mineralogy when the band is measured under simulated asteroid conditions, and can thus be used to determine a meteorite analog for remotely sensed hydrated asteroids. (Note: simulated asteroid conditions are under vacuum (<0.0001 mbar) at <125 K with samples heated from below Hanna et al., 2019.) But in their study finding thermal hydration as an explanation of spectral changes, Hiroi et al. (1996) did not use simulated asteroid conditions for their measurements, so it is not clear if thermal effects that cause band depth decreases can fully explain surface maturation trends on Ryugu. In addition, Kitazato et al. (2021) suggest that excursions sunward to create strong thermal effects are not consistent with thermodynamical models of Ryugu. Perhaps this is an area for further study: Are thermal processes more important on these asteroid surfaces than they are on ordinary chondrite parent bodies? Do thermal effects consistently cause reddening of the optical surface of a carbonaceous asteroid? Whatever the cause, a slightly deeper 2.7-micron band is observed after artificial crater formation and among returned samples from Ryugu, while essentially no difference is observed before and after artificial crater formation on Bennu (Fig. 12). Taken together, these comparisons may indicate that alteration of the 2.7 μm band is not a strong outcome of surface maturation on these dark asteroids. Artificial crater formation on both Bennu and Ryugu was associated with production of a cloud of fine particles that may have settled down close to the crater site. Thus it is possible that texture changes due to crater formation may be more important than exposure of the subsurface in explaining any resulting spectral changes (Nakauchi et al., 2021; Prince and Loeffler, 2022).

Models of divergent color evolution: The models presented by Trang et al. (2021) are particularly relevant at this juncture. The Thompson et al. (2020) study showed that space weathering of a hydrated substrate leads to magnetite formation. Hence, when included in the Trang et al. (2021) Hapke model, this magnetite causes spectral
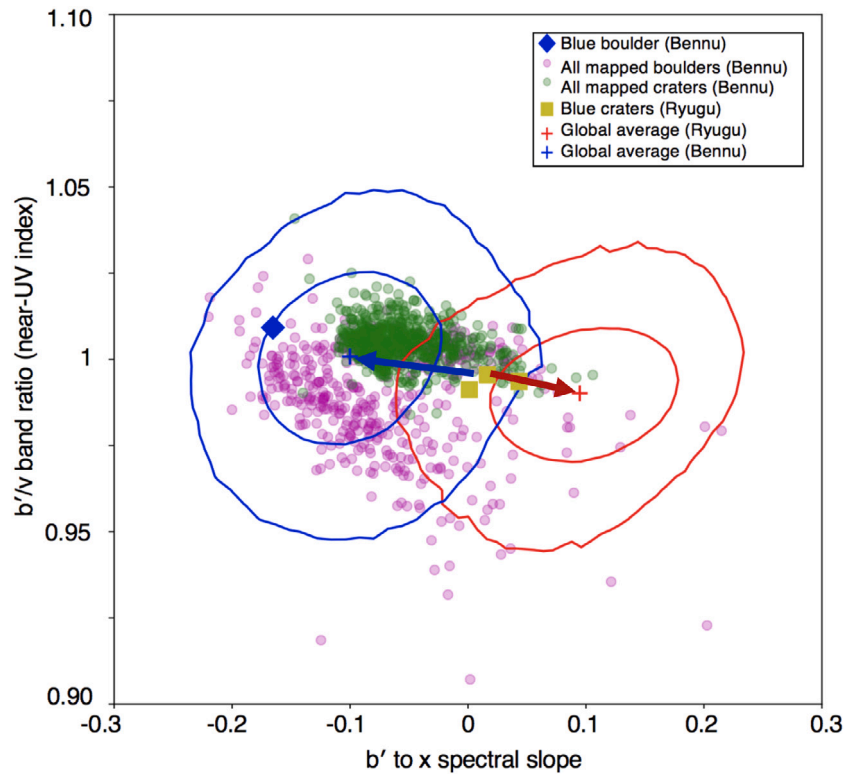
Fig. 11. This figure shows the imaging broadband visible wavelength b′/v ratio vs. b′ to x spectral slope global average parameter values, along with the colors of craters, for Bennu and Ryugu, compared with boulders on Bennu. While Fig. 10 shows an almost perfect match between Ryugu's bluest craters (above: light green squares), and Bennu's reddest craters (above: green filled circles), we indicate that the direction of maturation of color units toward global average, over time (based on relative age relationships), is toward the left on Bennu (blue arrow) and toward the right on Ryugu (red arrow). The concentric circles indicate the positions of 1 and 2-sigma standard deviations from the Ryugu average (red), and the Bennu average (blue) (from Supplementary Figure 14 in DellaGiustina et al. (2020)). (For interpretation of the references to color in this figure legend, the reader is referred to the web version of this article.)
Source: Adapted from DellaGiustina et al. (2020).

blueing, as in the case of Bennu, while space weathering of a dehydrated (or less hydrated) surface leads to iron formation (Lantz et al., 2017), and hence spectral reddening, as in the case of Ryugu. The Trang et al. models are thus consistent with the differences observed between Bennu and Ryugu, and can also be projected forward in time to explain reddening of Bennu equatorial materials that are old and partially dehydrated. Finally, the Trang et al. models are also consistent with the spectral effect findings from laboratory simulations of space weathering conducted by Hiroi et al. (2013), Lantz et al. (2017), Gillis-Davis et al. (2017), Nakamura et al. (2019), and Nakamura et al. (2020). However, not all experimental evidence supports this hypothesis (see Tables 1 and 2).

Physical properties of the substrate: The possibility that surface maturation depends on physical properties of the substrate that vary across the surface must also be examined. Such properties include porosity, cohesion, grain size, texture, thermal inertia, temperature, and age. Based on the published literature, we can summarize the physical properties of the surfaces on Bennu and Ryugu to see whether physical factors can explain some of the differences in maturation trends (Table 4). However, what we find is that most physical properties are shared by the two asteroid surfaces. Indeed, Table 4 indicates that Ryugu is, on average, similar to the dark (most abundant) boulders on Bennu in terms of thermophysical properties. We suggest that the only globally significant differences between Bennu and Ryugu are that (1) the thermal inertia and porosity of the brighter boulders contribute more to the global average values on Bennu than they do on Ryugu, and (2) dust cover appears to be more extensive on Ryugu than it is on Bennu, which might make sense as Ryugu is a larger body, and would

thus be able to retain more fine grains created by impacts. Perhaps relatedly, Hiroi et al. (2020) describe a CM meteorite analog for Ryugu that appears darker when measured as a (dust) powder than as a chip (this is also true for sulfides, but not true for most CCs), and Ryugu is slightly darker than Bennu.

Surface age: We can also compare the relative ages of surfaces on Bennu and Ryugu (Table 5). Bennu has a surface that is older than Ryugu: Bennu retains larger craters to about 10–65 Myr old (Bierhaus et al., 2022), while Ryugu retains larger craters up to 9 Myr old (Arakawa et al., 2020). Bennu's equator is enriched in the largest craters while showing the smallest gravitational slopes, indicating that the equator is old relative to the mid-latitudes (Bierhaus et al., 2022). In contrast, probably due to its different rotation state, Ryugu's surface material motion indicates that the mid-latitudes are older, while the equator and polar regions are more recently exposed (Sugita et al., 2019).

Equatorial bands: Bennu's equatorial materials are darker than average in laser altimeter studies at 1064 nm (Neumann et al., 2020), and in global photometry studies of the OVIRS spectra (Sen et al., 2021a; Zou et al., 2021), while they show little to no difference from average in visible wavelength imaging data studies (Golish et al., 2021; DellaGiustina et al., 2020). We interpret Figs. 6(a), 8, and 9 to indicate that Bennu's equator is darker than the mid-latitudes by approximately 10 ± 1% relative normal albedo at 1064 nm, but the observational bias imposed by the viewing and illumination conditions effectively hides this contrast at shorter wavelengths (Sen et al., 2021a; Zou et al., 2021; Li et al., 2021). Ryugu, on the other hand, shows a narrow equatorial band of materials that are brighter by about 9 ± 1% relative
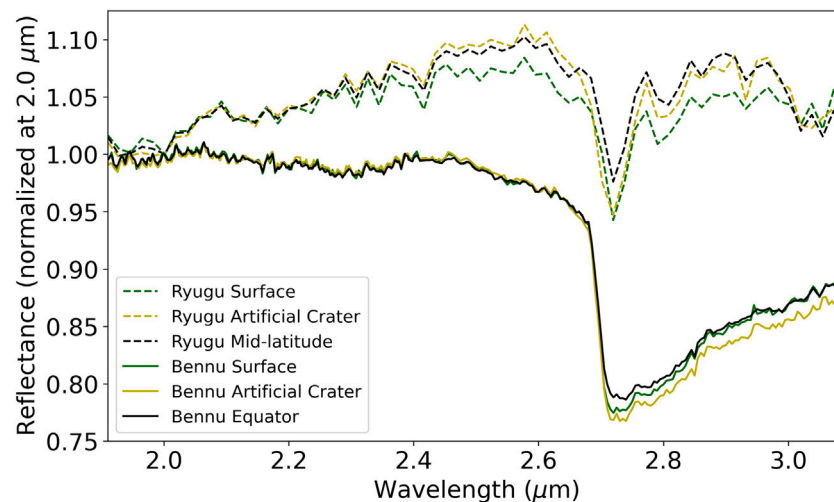
Fig. 12. Comparison of changes in spectra of the surface before and after artificial crater events on Bennu (solid lines) and Ryugu (dashed lines). Data for the crater that Hayabusa2 made on Ryugu were contributed by Kitazato et al. (2021), and data for the crater that OSIRIS-REx made on Bennu were contributed by Lauretta et al. (2022).

Table 4

Physical properties of asteroids Bennu and Ryugu, as ascertained by thermal observations and visible wavelength observations.

Property	Bennu	Ryugu
Thermal inertia	$330-370$ tiu (global avg.), $400-700$ tiu (bright boulders), $180-250$ tiu (dark boulders)[a]	$180-270$ tiu (global avg.)[d], $-$, 282^{+93}_{-35} tiu (dark boulder)[e]
Geometric albedo	0.044 ± 0.002[b]	0.040 ± 0.005[f]
Roughness	$(40 \pm 3)°$[a]	$(47 \pm 5)°$[d]
Dust cover	$<50\,\mu m$[a]	$<300\,\mu m$[g]
Dust particle size	$<65-100\,\mu m$[c]	$-$
Porosity	24–38% (bright boulders), 49–55% (dark boulders)[a]	41–55% (global avg.)[h]

[a]Rozitis et al. (2020).
[b]Golish et al. (2021).
[c]Hamilton et al. (2021).
[d]Shimaki et al. (2020).
[e]Grott et al. (2017).
[f]Tatsumi et al. (2020).
[g]Morota et al. (2020).
[h]Flynn et al. (2018).

Table 5

Relative ages of asteroids Bennu and Ryugu.

Timescale	Bennu	Ryugu
Global max. crater age	10–65 Myr[a]	6.4–11.4 Myr[c]
Equator	Older than average[a]	Younger than average[d]
Mid-latitudes	Younger than average[a]	Older than average[d]
Poles	Younger than average[a]	Younger than average[d,e]
Near-Earth residence age	1–2.5 Myr[b]	~8 Myr[f]

[a]As published by Bierhaus et al. (2022).
[b]As published by Ballouz et al. (2020).
[c]As published by Arakawa et al. (2020).
[d]As published by Sugita et al. (2019).
[e]As published by Tatsumi et al. (2021).
[f]As published by Morota et al. (2020).

normal albedo at 550 nm than the background (Yokota et al., 2021). However, Pilorget et al. (2021) show that the Ryugu data are also affected by the observational bias, forcing the lowest-incidence-angle observations to be along the equator. Thus, while the observational bias imposed by the spin states of these asteroids is working to hide Bennu's darkened equator, it is working to enhance Ryugu's brightened equator.

Movement towards or away from the equator: In parallel with albedo, the spectral characteristics of regions along the equator on Bennu are redder than the background (Fig. 6(b)) (Barucci et al., 2020), while color units detected along the equator of Ryugu are bluer than the background (Yokota et al., 2021). However, the results for Bennu and Ryugu (Barucci et al., 2019, 2020) show consistent color trends when the likely motion of material away or toward the equator is considered. The motion of material on Bennu is toward the equator (Scheeres et al., 2019; Jawin et al., 2020), and equatorial materials, possibly having older surface exposure ages, show redder spectra than background. On Ryugu materials seem to be moving away from the equator, towards mid-latitudes in the current epoch, and thus the mid-latitudes, having older surfaces exposure ages, show redder spectra than background average (Watanabe et al., 2019; Sugita et al., 2019; Yokota et al., 2021).

4. Conclusion: A working model for space weathering on Bennu

To summarize: Analyses of boulders and crater colors on Bennu suggest that the slope of Bennu's spectrum decreases (becomes bluer) with age. This is associated with an increase in albedo (brightening). In the older equatorial regions, however, where surface material concentrates at the geopotential low, there is a reddening and darkening trend, and a flattening of the hydration band at 2.7 μm, along with a possible shift

towards longer wavelengths. Mechanical breakdown, cratering, and mass wasting refresh the surface, acting to oppose the optical effects of maturation. OH creation due to H implantation is a possible result of solar wind bombardment, and this may work at cross-purposes with dehydration. However, since the hydration band is flattening along the equator, the timescale of OH creation from implantation appears to be slower than other (e.g. space weathering or thermal) processes that are attenuating the 2.7 μm band depth.

Synthesis model: We thus propose the following synthesis model for surface maturation on Bennu:

- Based on the comparison between Bennu and Ryugu, we suggest that the optical effects of maturation in the space environment depend on the level of hydration of the silicate/phyllosilicate substrate, as suggested by Lantz et al. (2017, 2018), and Trang et al. (2021).
- The physical properties of the regolith are similar on Bennu and Ryugu, hence do not cause the observed differences in weathering.
- Most albedo patterns on Bennu are due to compositional and/or morphological differences in surface boulders that probably trace back to the parent body (DellaGiustina et al., 2020).
- Very young craters on Bennu are redder than their surroundings due to smaller particle sizes from impacts (craters $<10-20\,m$), creation of fresh exposures of organics, or exposure of fresh unweathered subsurface (DellaGiustina et al., 2020; Lauretta et al., 2021).
- Intermediate age surfaces on Bennu are bluer and brighter due to solar wind or micrometeorite bombardment, possibly causing nanophase magnetite production (e.g. Trang et al. (2021) and DellaGiustina et al. (2020)), and/or dehydration maturation (e.g. Lantz et al. (2018)) that depends on substrate hydration state. Migration of fines away from the optical surface may also result in bluing.
- The very oldest surface at the equator of Bennu is redder (Li et al., 2021) and darker (Sen et al., 2021a; Neumann et al., 2020) and has a shallower hydroxyl absorption band (Praet et al., 2021; Simon et al., 2020b) due to nanophase iron opaque production (e.g. Trang et al. (2021) and Kaluna et al. (2016)).

Opaque production: We note that nanophase opaque production is a process that is known to occur on the Moon, and hence there are far more experiments in the published literature exploring this process (and what controls it) than for any other process. This imposes a bias when one searches for a laboratory study that can explain an observation. Nevertheless, nanophase and/or microphase opaque production are the favored explanations for some of the observations we have reviewed because, given the evidence examined in the paper, we have no logical reason for why particle size differences and/or carbon enrichment would be enhanced at the equator specifically. As shown in Fig. 6, the variations observed are not random as one might expect due to geologic processes on the surface of the asteroid. Instead, the color variations are strong functions of latitude. This is the evidence that points to space weathering processes, as they are known to be latitude-dependent (Hemingway et al., 2015).

Alternate models: An alternate explanation of the observations is that alteration of the optical surface of this asteroid due to exposure over time is too sensitively dependent on characteristics of the substrate (such as Fe/Mg silicate composition, density, porosity, age, thermal inertia, and temperature—in addition to hydration state) to allow a general description that explains all of the observations.

Or, perhaps, our observations can be synthesized into a cyclic maturation process: one which depends on the evolving composition and the compounds available for alteration. Solar wind is a constant process and likely dominates on young surfaces that have not had time to accumulate the effects of micrometeoroid impacts (because these are

stochastic). But, as a surface ages and is impacted by more micrometeoroids, those effects may become more prevalent. Impact simulations predict surfaces will blue. This may support an early reddening/late bluing effect. If the two processes are actually at odds with one another, depending on the overall effect of micrometeoroids, at later (older) stages, the surface may be oscillating between red and blue. Thus, in this scenario, we may have caught Ryugu in an early stage, and Bennu in a later, older stage—explaining why their spectral trends are different. In such a scenario, the hydration state of the target material would not be a predictive factor.

Final note: A full understanding awaits the analyses of fresh and space-weathered portions of returned samples. In particular, the contact pad samples on the TAGSAM head will be of great importance. The post-sampling images of the TAGSAM head (Lauretta et al., 2022) showed numerous particles trapped in several of the contact pads, and these particles will be among the best candidates for samples of the optical surface of Bennu, i.e., particles that were directly exposed to the space environment. In keeping with our working model, we propose the following testable hypotheses for surface maturation of Bennu returned samples:

Hypothesis 1. If exposure to the space environment modifies the spectral properties of Bennu's surface materials (DellaGiustina et al., 2020; Deshapriya et al., 2021; Lantz et al., 2018; Laczniak et al., 2020; Thompson et al., 2020) then samples will show that:

- Unweathered materials are spectrally redder in the VIS to NIR, brighter in the NIR, and darker and bluer in VIS wavelengths than average Bennu. The 2.7-μm absorption feature band minimum occurs at shorter wavelengths and has a sharper shape compared to weathered material.
- Mildly weathered materials are brighter in the near-UV wavelengths relative to the VIS-NIR than Bennu's average spectra. Mildly weathered materials are also brighter overall and more neutrally sloped than Bennu's average, while the 2.7-μm absorption band minimum occurs at longer wavelengths.
- The most highly weathered materials are redder and darker than average Bennu material in the NIR wavelengths. However, these materials are associated with the equatorial regions, and may not therefore be present in Nightingale samples.
- Mid-IR spectral changes will include reduced restrahlen band strength and shifts in band positions (Brunetto et al., 2020).

Hypothesis 2. If space weathering changes the chemistry and mineralogy of the regolith that is probed by remote sensing observations, then the samples will show that:

- Phyllosilicates are transformed to nanophase and microphase sulfides (troilite and pentlandite) and nanophase magnetite, with limited abundances of nanophase and microphase iron (Trang et al., 2021; Gillis-Davis et al., 2017; Thompson et al., 2019, 2020).
- Aliphatic organics are converted to aromatic molecules. Samples with an aliphatic spectral signature have space exposure ages less than a few million years (Kaplan et al., 2021; Thompson et al., 2020).

Hypothesis 3. If exposure to the space environment affects the uppermost layers of the regolith (Matsumoto et al., 2015), then individual sample particles may exhibit both space-weathered and unweathered surfaces and contain various amounts of implanted solar wind.

In conclusion, we are at the beginning of a remarkable decade of sample return from asteroids, linking laboratory analyses to remote-sensing data sets.

Declaration of competing interest

The authors declare that they have no known competing financial interests or personal relationships that could have appeared to influence the work reported in this paper.

Data availability

Data will be made available on request.

Acknowledgments

References

Adams, J.B., Jones, R.L., 1970. Spectral reflectivity of lunar samples. Science 167 (3918), 737–739.

Ammannito, E., DeSanctis, M., Ciarniello, M., Frigeri, A., Carrozzo, F., Combe, J.-P., Ehlmann, B., Marchi, S., McSween, H., Raponi, A., et al., 2016. Distribution of phyllosilicates on the surface of Ceres. Science 353 (6303), aaf4279.

Arakawa, M., Saiki, T., Wada, K., Ogawa, K., Kadono, T., Shirai, K., Sawada, H., Ishibashi, K., Honda, R., Sakatani, N., et al., 2020. An artificial impact on the asteroid (162173) Ryugu formed a crater in the gravity-dominated regime. Science 368 (6486), 67–71.

Ballouz, R.-L., Baresi, N., Crites, S.T., Kawakatsu, Y., Fujimoto, M., 2019. Surface refreshing of Martian moon Phobos by orbital eccentricity-driven grain motion. Nat. Geosci. 12 (4), 229–234.

Ballouz, R.-L., Walsh, K., Barnouin, O., DellaGiustina, D., Asad, M.A., Jawin, E., Daly, M., Bottke, W., Michel, P., Avdellidou, C., et al., 2020. Bennu's near-Earth lifetime of 1.75 million years inferred from craters on its boulders. Nature 587 (7833), 205–209.

Barnouin, O., Daly, M., Palmer, E., Gaskell, R., Weirich, J., Johnson, C., Al Asad, M., Roberts, J., Perry, M., Susorney, H., et al., 2019. Shape of (101955) Bennu indicative of a rubble pile with internal stiffness. Nat. Geosci. 12 (4), 247–252.

Barucci, M., Hasselmann, P., Fulchignoni, M., Honda, R., Yokota, Y., Sugita, S., Kitazato, K., Deshapriya, J., Perna, D., Tatsumi, E., et al., 2019. Multivariable statistical analysis of spectrophotometry and spectra of (162173) Ryugu as observed by JAXA Hayabusa2 mission. Astron. Astrophys. 629, A13.

Barucci, M., Hasselmann, P., Praet, A., Fulchignoni, M., Deshapriya, J., Fornasier, S., Merlin, F., Clark, B.E., Simon, A., Hamilton, V., et al., 2020. OSIRIS-REx spectral analysis of (101955) Bennu by multivariate statistics. Astron. Astrophys. 637, L4.

Beck, P., Quirico, E., Montes-Hernandez, G., Bonal, L., Bollard, J., Orthous-Daunay, F.-R., Howard, K., Schmitt, B., Brissaud, O., Deschamps, F., et al., 2010. Hydrous mineralogy of CM and CI chondrites from infrared spectroscopy and their relationship with low albedo asteroids. Geochim. Cosmochim. Acta 74 (16), 4881–4892.

Bennett, C., DellaGiustina, D., Becker, K., Becker, T., Edmundson, K., Golish, D., Bennett, R., Burke, K., Cue, C., Clark, B.E., et al., 2021. A high-resolution global basemap of (101955) Bennu. Icarus 357, 113690.

Bierhaus, E., Trang, D., Daly, R., Bennett, C., Barnouin, O., Walsh, K., Ballouz, R.-L., Bottke, W., Burke, K., Perry, M., et al., 2022. Crater population on asteroid (101955) Bennu indicates impact armouring and a young surface. Nat. Geosci. 15, 440–446.

Binzel, R.P., DeMeo, F.E., Burt, B.J., Cloutis, E.A., Rozitis, B., Burbine, T.H., Campins, H., Clark, B.E., Emery, J.P., Hergenrother, C.W., et al., 2015. Spectral slope variations for OSIRIS-REx target asteroid (101955) Bennu: possible evidence for a fine-grained regolith equatorial ridge. Icarus 256, 22–29.

Bonal, L., Brunetto, R., Beck, P., Dartois, E., Dionnet, Z., Djouadi, Z., Duprat, J., Füri, E., Kakazu, Y., Montagnac, G., et al., 2015. Visible-IR and Raman microspectroscopic investigation of three Itokawa particles collected by Hayabusa: Mineralogy and degree of space weathering based on nondestructive analyses. Meteorit. Planet. Sci. 50 (9), 1562–1576.

Bottke, W., Moorhead, A., Connolly Jr., H., Hergenrother, C., Molaro, J., Michel, P., Nolan, M., Schwartz, S., Vokrouhlický, D., Walsh, K., et al., 2020. Meteoroid impacts as a source of Bennu's particle ejection events. J. Geophys. Res.: Planets 125 (8), e2019JE006282.

Brunetto, R., Lantz, C., Ledu, D., Baklouti, D., Barucci, M., Beck, P., Delauche, L., Dionnet, Z., Dumas, P., Duprat, J., et al., 2014. Ion irradiation of Allende meteorite probed by visible, IR, and Raman spectroscopies. Icarus 237, 278–292.

Brunetto, R., Lantz, C., Nakamura, T., Baklouti, D., Le Pivert-Jolivet, T., Kobayashi, S., Borondics, F., 2020. Characterizing irradiated surfaces using IR spectroscopy. Icarus 113722.

Brunetto, R., Loeffler, M.J., Nesvorný, D., Sasaki, S., Strazzulla, G., 2015. Asteroid surface alteration by space weathering processes. In: Asteroids IV. University of Arizona Press, Tucson, Arizona, pp. 597–616.

Burke, K.N., DellaGiustina, D.N., Bennett, C.A., Walsh, K.J., Pajola, M., Bierhaus, E.B., Nolan, M.C., Boynton, W.V., Brodbeck, J.I., Connolly, H.C., et al., 2021. Particle size-frequency distributions of the osiris-rex candidate sample sites on asteroid (101955) bennu. Remote Sens. 13 (7), 1315.

Cambioni, S., Delbo, M., Poggiali, G., Avdellidou, C., Ryan, A., Deshapriya, J., Asphaug, E., Ballouz, R.-L., Barucci, M., Bennett, C., et al., 2021. Fine-regolith production on asteroids controlled by rock porosity. Nature 598 (7879), 49–52.

Campins, H., de León, J., Licandro, J., Hendrix, A., Sánchez, J.A., Ali-Lagoa, V., 2018. Compositional diversity among primitive asteroids. In: Primitive Meteorites and Asteroids. Elsevier, pp. 345–369.

Cassidy, W., Hapke, B., 1975. Effects of darkening processes on surfaces of airless bodies. Icarus 25 (3), 371–383.

Christensen, P.R., Hamilton, V.E., Mehall, G., Pelham, D., O'Donnell, W., Anwar, S., Bowles, H., Chase, S., Fahlgren, J., Farkas, Z., et al., 2018. The OSIRIS-REx thermal emission spectrometer (OTES) instrument. Space Sci. Rev. 214 (5), 1–39.

Christoffersen, R., Keller, L., 2015. Solar ion processing of itokawa grains: Constraints on surface exposure times. In: Lunar and Planetary Science Conference, JSC-CN-32917.

Clark, B.E., 2022. Opening the Ryugu sample capsule. Nat. Astron. 6 (2), 180–181.

Clark, B.E., Binzel, R.P., Howell, E.S., Cloutis, E.A., Ockert-Bell, M., Christensen, P., Barucci, M.A., DeMeo, F., Lauretta, D.S., Connolly Jr., H., et al., 2011. Asteroid (101955) 1999 RQ36: Spectroscopy from 0.4 to 2.4 μm and meteorite analogs. Icarus 216 (2), 462–475.

Clark, B.E., Hapke, B., Pieters, C., Britt, D., 2002. Asteroid space weathering and regolith evolution. In: Asteroids III, Vol. 585. Citeseer, 90086–2.

Cloutis, E., Hiroi, T., Gaffey, M., Alexander, C.O., Mann, P., 2011. Spectral reflectance properties of carbonaceous chondrites: 1. CI chondrites. Icarus 212 (1), 180–209.

Cloutis, E.A., Pietrasz, V.B., Kiddell, C., Izawa, M.R., Vernazza, P., Burbine, T.H., DeMeo, F., Tait, K.T., Bell III, J.F., Mann, P., et al., 2018. Spectral reflectance "deconstruction" of the Murchison CM2 carbonaceous chondrite and implications for spectroscopic investigations of dark asteroids. Icarus 305, 203–224.

Daly, M., Barnouin, O., Dickinson, C., Seabrook, J., Johnson, C., Cunningham, G., Haltigin, T., Gaudreau, D., Brunet, C., Aslam, I., et al., 2017. The OSIRIS-REx laser altimeter (OLA) investigation and instrument. Space Sci. Rev. 212 (1), 899–924.

Daly, M., Barnouin, O., Seabrook, J., Roberts, J., Dickinson, C., Walsh, K., Jawin, E., Palmer, E., Gaskell, R., Weirich, J., et al., 2020. Hemispherical differences in the shape and topography of asteroid (101955) Bennu. Sci. Adv. 6 (41), eabd3649.

Delbo, M., Walsh, K.J., Matonti, C., Wilkerson, J., Pajola, M., Al Asad, M.M., Avdellidou, C., Ballouz, R.-L., Bennett, C.A., Connolly, H.C., et al., 2022. Alignment of fractures on Bennu's boulders indicative of rapid asteroid surface evolution. Nat. Geosci. 15, 453–457.

DellaGiustina, D., Burke, K., Walsh, K., Smith, P., Golish, D., Bierhaus, E., Ballouz, R.-L., Becker, T., Campins, H., Tatsumi, E., Yumoto, K., Sugita, S., Deshapriya, J., Cloutis, E., Clark, B.E., Hendrix, A., Sen, A., Al Asad, M., Daly, M., Applin, D., Avdellidou, C., Barucci, M., Becker, K., Bennett, C., Bottke, W., Brodbeck, J., Connolly, H., Delbo, M., de Leon, J., Drouet d'Aubigny, C., Edmundson, K., Fornasier, S., Hamilton, V., Hasselmann, P., Hergenrother, C., Howell, E., Jawin, E., Kaplan, H., Le Corre, L., Lim, L., Li, J.-Y., Michel, P., Molaro, J., Nolan, M., Nolau, J., Pajola, M., Parkinson, A., Popescu, M., Porter, N., Rizk, B., Rizos, J., Ryan, A., Rozitis, B., Shultz, N., Simon, A., Trang, D., Van Auken, R., Wolner, C., Lauretta, D., 2020. Variations in color and reflectance on the surface of asteroid (101955) Bennu. Science 370 (6517), eabc3660.

DellaGiustina, D., Emery, J., Golish, D., Rozitis, B., Bennett, C., Burke, K., Ballouz, R.-L., Becker, K., Christensen, P., d'Aubigny, C.D., et al., 2019. Properties of rubble-pile asteroid (101955) Bennu from OSIRIS-REx imaging and thermal analysis. Nat. Astron. 3 (4), 341–351.

Deshapriya, J., Barucci, M., Bierhaus, E., Fornasier, S., Hasselmann, P., Merlin, F., Clark, B.E., Praet, A., Fulchignoni, M., Simon, A., et al., 2021. Spectral analysis of craters on (101955) Bennu. Icarus 357, 114252.

Ferrone, S., Clark, B.E., Kaplan, H., Rizos, J.-L., Zou, X.-D., Li, J.-Y., Barucci, M., Simon, A., Reuter, D., Hasselmann, P., et al., 2021. Visible–near-infrared observations of organics and carbonates on (101955) Bennu: Classification method and search for surface context. Icarus 368, 114579.

Flynn, G.J., Consolmagno, G.J., Brown, P., Macke, R.J., 2018. Physical properties of the stone meteorites: Implications for the properties of their parent bodies. Geochemistry 78 (3), 269–298.

Fornasier, S., Hasselmann, P., Deshapriya, J.P., Barucci, M., Clark, B.E., Praet, A., Hamilton, V., Simon, A., Li, J.-Y., Cloutis, E., et al., 2020. Phase reddening on asteroid Bennu from visible and near-infrared spectroscopy. Astron. Astrophys. 644, A142.

Fornasier, S., Lantz, C., Perna, D., Campins, H., Barucci, M., Nesvorny, D., 2016. Spectral variability on primitive asteroids of the Themis and Beagle families: Space weathering effects or parent body heterogeneity? Icarus 269, 1–14.

Gaffey, M.J., 2010. Space weathering and the interpretation of asteroid reflectance spectra. Icarus 209 (2), 564–574.

Gallant, J., Gladman, B., Ćuk, M., 2009. Current bombardment of the Earth–Moon system: Emphasis on cratering asymmetries. Icarus 202 (2), 371–382.

Garenne, A., Beck, P., Montes-Hernandez, G., Brissaud, O., Schmitt, B., Quirico, E., Bonal, L., Beck, C., Howard, K., 2016. Bidirectional reflectance spectroscopy of carbonaceous chondrites: Implications for water quantification and primary composition. Icarus 264, 172–183.

Gillis-Davis, J.J., Lucey, P.G., Bradley, J.P., Ishii, H.A., Kaluna, H.M., Misra, A., Connolly, Jr., H.C., 2017. Incremental laser space weathering of Allende reveals non-lunar like space weathering effects. Icarus 286, 1–14.

Gold, T., 1955. The lunar surface. Mon. Not. R. Astron. Soc. 115 (6), 585–604.

Golish, D., d'Aubigny, C.D., Rizk, B., DellaGiustina, D., Smith, P., Becker, K., Shultz, N., Stone, T., Barker, M., Mazarico, E., et al., 2020. Ground and in-flight calibration of the OSIRIS-REx Camera Suite. Space Sci. Rev. 216 (1), 1–31.

Golish, D., DellaGiustina, D., Li, J.-Y., Clark, B.E., Zou, X.-D., Smith, P., Rizos, J., Hasselmann, P., Bennett, C., Fornasier, S., et al., 2021. Disk-resolved photometric modeling and properties of asteroid (101955) Bennu. Icarus 357, 113724.

Grott, M., Knollenberg, J., Borgs, B., Hänschke, F., Kessler, E., Helbert, J., Maturilli, A., Müller, N., 2017. The MASCOT radiometer MARA for the Hayabusa 2 mission. Space Sci. Rev. 208 (1–4), 413–431.

Hamilton, V., Christensen, P., Kaplan, H., Haberle, C., Rogers, A., Glotch, T., Breitenfeld, L., Goodrich, C., Schrader, D., McCoy, T., et al., 2021. Evidence for limited compositional and particle size variation on asteroid (101955) Bennu from thermal infrared spectroscopy. Astron. Astrophys. 650, A120.

Hamilton, V.E., Kaplan, H.H., Connolly Jr., H.C., Goodrich, C.A., Abreu, N.M., Simon, A.A., 2022. GRO 95577 (CR1) as a mineralogical analogue for asteroid (101955) Bennu. Icarus 383, 115054.

Hamilton, V., Simon, A., Christensen, P., Reuter, D., Clark, B.E., Barucci, M., Bowles, N., Boynton, W., Brucato, J.R., Cloutis, E., et al., 2019. Evidence for widespread hydrated minerals on asteroid (101955) Bennu. Nat. Astron. 3 (4), 332–340.

Hanna, K.D., Schrader, D., Cloutis, E., Cody, G., King, A., McCoy, T., Applin, D., Mann, J., Bowles, N., Brucato, J., et al., 2019. Spectral characterization of analog samples in anticipation of OSIRIS-REx's arrival at Bennu: A blind test study. Icarus 319, 701–723.

Hapke, B., 2001. Space weathering from Mercury to the asteroid belt. J. Geophys. Res.: Planets 106 (E5), 10039–10073.

Hartzell, C.M., Scheeres, D.J., 2013. Dynamics of levitating dust particles near asteroids and the Moon. J. Geophys. Res.: Planets 118 (1), 116–125.

Hemingway, D.J., Garrick-Bethell, I., Kreslavsky, M.A., 2015. Latitudinal variation in spectral properties of the lunar maria and implications for space weathering. Icarus 261, 66–79.

Hendrix, A.R., Vilas, F., 2019. C-complex asteroids: UV-visible spectral characteristics and implications for space weathering effects. Geophys. Res. Lett. 46 (24), 14307–14317.

Hergenrother, C., Adam, C., Chesley, S., Lauretta, D., 2020. Introduction to the special issue: exploration of the activity of asteroid (101955) Bennu. J. Geophys. Res.: Planets 125 (9), e2020JE006549.

Hiroi, T., Milliken, R., Robertson, K., Kaiden, H., Misawa, K., Shimana, R., Sasaki, S., Matsuoka, M., Nakamura, T., Kitazato, K., et al., 2020. Meteorite hills 00639 as an analogue of asteroid 162173 Ryugu based on space weathering simulations of carbonaceous chondrites. In: Lunar and Planetary Science Conference, 2326. p. 1043.

Hiroi, T., Pieters, C., Zolensky, M., Prinz, M., 1996. Reflectance spectra (UV-3 micrometers) of heated Ivuna (CI) meteorite and newly identified thermally metamorphosed CM chondrites. In: Lunar and Planetary Science Conference, Vol. 27.

Hiroi, T., Sasaki, S., Misu, T., Nakamura, T., 2013. Keys to detect space weathering on Vesta: changes of visible and near-infrared reflectance spectra of HEDs and carbonaceous chondrites. In: 44th Annual Lunar and Planetary Science Conference, 1719. p. 1276.

Ishikawa, W., Sato, S., 2020. Mechanical C- C bond formation by laser driven shock wave. ChemPhysChem 21 (18), 2104.

Jawin, E., Walsh, K., Barnouin, O., McCoy, T., Ballouz, R.-L., DellaGiustina, D., Connolly Jr., H., Marshall, J., Beddingfield, C., Nolan, M., et al., 2020. Global patterns of recent mass movement on asteroid (101955) Bennu. J. Geophys. Res.: Planets 125 (9), e2020JE006475.

Jedicke, R., Nesvornỳ, D., Whiteley, R., Ivezić, Ž., Jurić, M., 2004. An age–colour relationship for main-belt S-complex asteroids. Nature 429 (6989), 275–277.

Johnson, T., Fanale, F., 1973. Optical properties of carbonaceous chondrites and their relationship to asteroids. J. Geophys. Res. 78, 8507–8518.

Kaiden, H., Hiroi, T., Misawa, K., Tanaka, H., Sasaki, S., Robertson, K., Milliken, R., Masai, H., Terao, J., 2019. Space weathering of olivine and the murchison CM2 carbonaceous chondrite simulated by ultraviolet irradiation. In: 50th Annual Lunar and Planetary Science Conference, 2132. p. 2630.

Kaluna, H., Ishii, H., Bradley, J., Gillis-Davis, J., Lucey, P., 2017. Simulated space weathering of Fe-and Mg-rich aqueously altered minerals using pulsed laser irradiation. Icarus 292, 245–258.

Kaluna, H.M., Masiero, J.R., Meech, K.J., 2016. Space weathering trends among carbonaceous asteroids. Icarus 264, 62–71.

Kaplan, H., Lauretta, D., Simon, A., Hamilton, V., DellaGiustina, D., Golish, D., Reuter, D., Bennett, C., Burke, K., Campins, H., et al., 2020. Bright carbonate veins on asteroid (101955) Bennu: Implications for aqueous alteration history. Science 370 (6517), eabc3557.

Kaplan, H., Simon, A., Hamilton, V., Thompson, M., Sandford, S., Barucci, M., Cloutis, E., Brucato, J., Reuter, D., Glavin, D., et al., 2021. Composition of organics on asteroid (101955) Bennu. Astron. Astrophys. 653, L1.

Keller, L.P., Berger, E.L., 2014. A transmission electron microscope study of Itokawa regolith grains. Earth Planets Space 66 (1), 1–7.

Keller, L.P., Berger, E.L., 2017. Transmission Electron Microscopy of Plagioclase-Rich Itokawa Grains: Space Weathering Effects and Solar Flare Track Exposure Ages, JSC-E-DAA-TN48810.

Keller, L., Christoffersen, R., Dukes, C., Baragiola, R., Rahman, Z., 2015. Ion irradiation experiments on the Murchison CM2 carbonaceous chondrite: Simulating space weathering of primitive asteroids. In: Johnson Space Center - Contribution Number 32777.

Kitazato, K., Milliken, R., Iwata, T., Abe, M., Ohtake, M., Matsuura, S., Arai, T., Nakauchi, Y., Nakamura, T., Matsuoka, M., et al., 2019. The surface composition of asteroid 162173 Ryugu from Hayabusa2 near-infrared spectroscopy. Science 364 (6437), 272–275.

Kitazato, K., Milliken, R., Iwata, T., Abe, M., Ohtake, M., Matsuura, S., Takagi, Y., Nakamura, T., Hiroi, T., Matsuoka, M., et al., 2021. Thermally altered subsurface material of asteroid (162173) Ryugu. Nat. Astron. 5 (3), 246–250.

Laczniak, D., Thompson, M., Christoffersen, R., Dukes, C., Clemett, S., Morris, R., Keller, L., 2021. Characterizing the spectral, microstructural, and chemical effects of solar wind irradiation on the Murchison carbonaceous chondrite through coordinated analyses. Icarus 364, 114479.

Laczniak, D., Thompson, M., Dukes, C., Morris, R., Clemett, S., Keller, L., Christoffersen, R., 2019. Coordinated analysis of an ion irradiated carbonaceous chondrite. In: 82nd Annual Meeting of the Meteoritical Society, Vol. 82. p. 6434.

Laczniak, D., Thompson, M., Dukes, C., Morris, R., Clemett, S., Keller, L., Christoffersen, R., 2020. Preparing for C-complex asteroid sample return: Investigating space weathering effects using coordinated analysis of a He+-and H+-irradiated carbonaceous chondrite. In: Lunar and Planetary Science Conference, 2326. p. 2667.

Lantz, C., Binzel, R., DeMeo, F., 2018. Space weathering trends on carbonaceous asteroids: A possible explanation for Bennu's blue slope? Icarus 302, 10–17.

Lantz, C., Brunetto, R., Barucci, M., Dartois, E., Duprat, J., Engrand, C., Godard, M., Ledu, D., Quirico, E., 2015. Ion irradiation of the Murchison meteorite: Visible to mid-infrared spectroscopic results. Astron. Astrophys. 577, A41.

Lantz, C., Brunetto, R., Barucci, M., Fornasier, S., Baklouti, D., Bourçois, J., Godard, M., 2017. Ion irradiation of carbonaceous chondrites: A new view of space weathering on primitive asteroids. Icarus 285, 43–57.

Lantz, C., Clark, B.E., Barucci, M., Lauretta, D., 2013. Evidence for the effects of space weathering spectral signatures on low albedo asteroids. Astron. Astrophys. 554, A138.

Lantz, C., Hamilton, V., Brunetto, R., Hanna, R., Christensen, P., Lauretta, D., 2020. Can we detect space weathering on bennu using OTES data? In: Lunar and Planetary Science Conference, 2326. p. 1850.

Lauretta, D., Adam, C., Allen, A., Ballouz, R.-L., Barnouin, O., Becker, K., Becker, T., Bennett, C., Bierhaus, E., Bos, B., et al., 2022. Spacecraft sample collection and subsurface excavation of asteroid (101955) Bennu. Science 377 (6603), 285–291.

Lauretta, D., Balram-Knutson, S., Beshore, E., Boynton, W., d'Aubigny, C.D., DellaGiustina, D., Enos, H., Golish, D., Hergenrother, C., Howell, E., et al., 2017. OSIRIS-REx: sample return from asteroid (101955) Bennu. Space Sci. Rev. 212 (1), 925–984.

Lauretta, D.S., Enos, H.L., Polit, A.T., Roper, H.L., Wolner, C.W., 2021. OSIRIS-REx at Bennu: Overcoming challenges to collect a sample of the early Solar System. In: Sample Return Missions. Elsevier, pp. 163–194.

Lauretta, D., Hergenrother, C., Chesley, S., Leonard, J., Pelgrift, J., Adam, C., Al Asad, M., Antreasian, P., Ballouz, R.-L., Becker, K., et al., 2019. Episodes of particle ejection from the surface of the active asteroid (101955) Bennu. Science 366 (6470), eaay3544.

Lazzarin, M., Marchi, S., Moroz, L., Brunetto, R., Magrin, S., Paolicchi, P., Strazzulla, G., 2006. Space weathering in the main asteroid belt: The big picture. Astrophys. J. Lett. 647 (2), L179.

Lee, P., 1996. Dust levitation on asteroids. Icarus 124 (1), 181–194.

Lee, M.R., Lindgren, P., King, A.J., Greenwood, R.C., Franchi, I.A., Sparkes, R., 2016. Elephant Moraine 96029, a very mildly aqueously altered and heated CM carbonaceous chondrite: Implications for the drivers of parent body processing. Geochim. Cosmochim. Acta 187, 237–259.

Li, J.-Y., Helfenstein, P., Buratti, B., Takir, D., Clark, B.E., 2015. Asteroid photometry. In: Asteroids IV, Vol. 86. University of Arizona Press, pp. 277–326.

Li, J.-Y., Zou, X.-D., Golish, D.R., Clark, B.E., Ferrone, S., Fornasier, S., Hasselmann, P.H., Ryan, A.J., Rozitis, B., Emery, J.P., et al., 2021. Spectrophotometric modeling and mapping of (101955) bennu. Planet. Sci. J. 2 (3), 117.

Loeffler, M., Dukes, C., Baragiola, R., 2009. Irradiation of olivine by 4 keV He+: Simulation of space weathering by the solar wind. J. Geophys. Res.: Planets 114 (E3).

Lucey, P., Neumann, G., Riner, M., Mazarico, E., Smith, D., Zuber, M., Paige, D., Bussey, D., Cahill, J., McGovern, A., et al., 2014. The global albedo of the Moon at 1064 nm from LOLA. J. Geophys. Res.: Planets 119 (7), 1665–1679.

Marchi, S., Paolicchi, P., Richardson, D., 2012. Collisional evolution and reddening of asteroid surfaces–I. The problem of conflicting time-scales and the role of size-dependent effects. Mon. Not. R. Astron. Soc. 421 (1), 2–8.

Matsumoto, T., Tsuchiyama, A., Miyake, A., Noguchi, T., Nakamura, M., Uesugi, K., Takeuchi, A., Suzuki, Y., Nakano, T., 2015. Surface and internal structures of a space-weathered rim of an Itokawa regolith particle. Icarus 257, 230–238.

Matsuoka, M., Nakamura, T., Hiroi, T., Okumura, S., Sasaki, S., 2020. Space weathering simulation with low-energy laser irradiation of Murchison CM chondrite for reproducing micrometeoroid bombardments on C-type asteroids. Astrophys. J. Lett. 890 (2), L23.

Matsuoka, M., Nakamura, T., Kimura, Y., Hiroi, T., Nakamura, R., Okumura, S., Sasaki, S., 2015. Pulse-laser irradiation experiments of Murchison CM2 chondrite for reproducing space weathering on C-type asteroids. Icarus 254, 135–143.

Merlin, F., Deshapriya, J., Fornasier, S., Barucci, M., Praet, A., Hasselmann, P., Clark, B.E., Hamilton, V., Simon, A., Reuter, D., et al., 2021. In search of Bennu analogs: Hapke modeling of meteorite mixtures. Astron. Astrophys. 648, A88.

Milliken, R.E., Mustard, J.F., 2005. Quantifying absolute water content of minerals using near-infrared reflectance spectroscopy. J. Geophys. Res.: Planets 110 (E12).

Milliken, R.E., Mustard, J.F., 2007. Estimating the water content of hydrated minerals using reflectance spectroscopy: I. Effects of darkening agents and low-albedo materials. Icarus 189 (2), 550–573.

Miyamoto, H., Yano, H., Scheeres, D.J., Abe, S., Barnouin-Jha, O., Cheng, A.F., Demura, H., Gaskell, R.W., Hirata, N., Ishiguro, M., et al., 2007. Regolith migration and sorting on asteroid Itokawa. Science 316 (5827), 1011–1014.

Molaro, J.L., Hergenrother, C.W., Chesley, S., Walsh, K.J., Hanna, R.D., Haberle, C.W., Schwartz, S.R., Ballouz, R.-L., Bottke, W., Campins, H., et al., 2020b. Thermal fatigue as a driving mechanism for activity on asteroid Bennu. J. Geophys. Res.: Planets 125 (8), e2019JE006325.

Molaro, J., Walsh, K., Jawin, E., Ballouz, R.-L., Bennett, C., DellaGiustina, D., Golish, D., d'Aubigny, C.D., Rizk, B., Schwartz, S., et al., 2020a. In situ evidence of thermally induced rock breakdown widespread on Bennu's surface. Nature Commun. 11 (1), 1–11.

Moore, C.B., Lewis, C.F., 1967. Total carbon content of ordinary chondrites. J. Geophys. Res. 72 (24), 6289–6292.

Morota, T., Sugita, S., Cho, Y., Kanamaru, M., Tatsumi, E., Sakatani, N., Honda, R., Hirata, N., Kikuchi, H., Yamada, M., et al., 2020. Sample collection from asteroid (162173) Ryugu by Hayabusa2: Implications for surface evolution. Science 368 (6491), 654–659.

Moroz, L., Arnold, G., Korochantsev, A., Wäsch, R., 1998. Natural solid bitumens as possible analogs for cometary and asteroid organics:: 1. reflectance spectroscopy of pure bitumens. Icarus 134 (2), 253–268.

Moroz, L., Baratta, G., Strazzulla, G., Starukhina, L., Dotto, E., Barucci, M.A., Arnold, G., Distefano, E., 2004a. Optical alteration of complex organics induced by ion irradiation:. 1. Laboratory experiments suggest unusual space weathering trend. Icarus 170 (1), 214–228.

Moroz, L., Hiroi, T., Shingareva, T., Basilevsky, A., Fisenko, A., Semjonova, L., Pieters, C., 2004b. Reflectance spectra of CM2 chondrite Mighei irradiated with pulsed laser and implications for low-albedo asteroids and Martian moons. In: Lunar and Planetary Science Conference. p. 1279.

Nakamura, A.M., Fujiwara, A., Kadono, T., 1994. Velocity of finer fragments from impact. Planet. Space Sci. 42 (12), 1043–1052.

Nakamura, T., Lantz, C., Kobayashi, S., Nakauchi, Y., Amano, K., Brurnetto, R., Matsumoto, M., Takahashi, M., Matsuoka, M., Noguchi, T., et al., 2019. Experimental reproduction of space weathering of C-type asteroids by he exposure to shocked and partially dehydrated carbonaceous chondrites. In: 82nd Annual Meeting of the Meteoritical Society, Vol. 82. p. 6211.

Nakamura, T., Lantz, C., Nakauchi, Y., Amano, K., Brurnetto, R., Matsumoto, M., Kobayashi, S., Matsuoka, M., Noguchi, T., Matsumoto, T., Zolensky, M.E., 2020. Irradiation-energy dependence on the spectral changes of hydrous C-type asteroids based on 4keV and 20keV he exposure experiments of murchison CM chondrite. In: Lunar and Planetary Science Conference. In: Lunar and Planetary Science Conference, p. 1310.

Nakauchi, Y., Abe, M., Ohtake, M., Matsumoto, T., Tsuchiyama, A., Kitazato, K., Yasuda, K., Suzuki, K., Nakata, Y., 2021. The formation of H2O and Si-OH by H2+ irradiation in major minerals of carbonaceous chondrites. Icarus 355, 114140.

Nesvornỳ, D., Bottke, W.F., VokrouhlickÝ, D., Sykes, M., Lien, D.J., Stansberry, J., 2008. Origin of the near-ecliptic circumsolar dust band. Astrophys. J. Lett. 679 (2), L143.

Nesvornỳ, D., Jedicke, R., Whiteley, R.J., Ivezić, Ž., 2005. Evidence for asteroid space weathering from the Sloan Digital Sky Survey. Icarus 173 (1), 132–152.

Neumann, G., Barker, M., Mazarico, E., Daly, M., Barnouin, O., Jawin, E., Lauretta, D., 2020. Global and local variations in 1064-nm normal albedo of Bennu from the OSIRIS-REx laser altimeter. In: 51st Annual Lunar and Planetary Science Conference, 2326. p. 2032.

Neumann, G.A., Cavanaugh, J.F., Sun, X., Mazarico, E.M., Smith, D.E., Zuber, M.T., Mao, D., Paige, D.A., Solomon, S.C., Ernst, C.M., et al., 2013. Bright and dark polar deposits on Mercury: Evidence for surface volatiles. Science 339 (6117), 296–300.

Noble, S.K., Pieters, C.M., Keller, L.P., 2007. An experimental approach to understanding the optical effects of space weathering. Icarus 192 (2), 629–642.

Noguchi, T., Kimura, M., Hashimoto, T., Konno, M., Nakamura, T., Zolensky, M.E., Okazaki, R., Tanaka, M., Tsuchiyama, A., Nakato, A., et al., 2014. Space weathered rims found on the surfaces of the Itokawa dust particles. Meteorit. Planet. Sci. 49 (2), 188–214.

Pearson, V., Sephton, M., Franchi, I., Gibson, J., Gilmour, I., 2006. Carbon and nitrogen in carbonaceous chondrites: Elemental abundances and stable isotopic compositions. Meteorit. Planet. Sci. 41 (12), 1899–1918.

Pieters, C.M., Taylor, L.A., Noble, S.K., Keller, L.P., Hapke, B., Morris, R.V., Allen, C.C., McKAY, D.S., Wentworth, S., 2000. Space weathering on airless bodies: Resolving a mystery with lunar samples. Meteorit. Planet. Sci. 35 (5), 1101–1107.

Pilorget, C., Fernando, J., Riu, L., Kitazato, K., Iwata, T., 2021. Global-scale albedo and spectro-photometric properties of Ryugu from NIRS3/Hayabusa2, implications for the composition of Ryugu and the representativity of the returned samples. Icarus 355, 114126.

Pilorget, C., Okada, T., Hamm, V., Brunetto, R., Yada, T., Loizeau, D., Riu, L., Usui, T., Moussi-Soffys, A., Hatakeda, K., et al., 2022. First analyses by MicrOmega of the samples returned to Earth by the Hayabusa2 mission. Nat. Astron. 6, 221–225.

Praet, A., Barucci, M., Clark, B.E., Kaplan, H., Simon, A., Hamilton, V., Emery, J., Howell, E., Lim, L., Zou, X.-D., et al., 2021. Hydrogen abundance estimation and distribution on (101955) Bennu. Icarus 363, 114427.

Prince, B., Loeffler, M., 2022. Space weathering of the 3-μm phyllosilicate feature induced by pulsed laser irradiation. Icarus 372, 114736.

Reuter, D., Simon, A., Hair, J., Lunsford, A., Manthripragada, S., Bly, V., Bos, B., Brambora, C., Caldwell, E., Casto, G., et al., 2018. The OSIRIS-REx Visible and InfraRed spectrometer (OVIRS): spectral maps of the asteroid Bennu. Space Sci. Rev. 214 (2), 54.

Rizk, B., d'Aubigny, C.D., Golish, D., Fellows, C., Merrill, C., Smith, P., Walker, M., Hendershot, J., Hancock, J., Bailey, S., et al., 2018. OCAMS: the OSIRIS-REx camera suite. Space Sci. Rev. 214 (1), 1–55.

Rizos, J., de León, J., Licandro, J., Golish, D., Campins, H., Tatsumi, E., Popescu, M., DellaGiustina, D., Pajola, M., Li, J.-Y., et al., 2021. Bennu's global surface and two candidate sample sites characterized by spectral clustering of OSIRIS-REx multispectral images. Icarus 364, 114467.

Rozitis, B., Ryan, A., Emery, J., Christensen, P., Hamilton, V., Simon, A., Reuter, D., Al Asad, M., Ballouz, R.-L., Bandfield, J., et al., 2020. Asteroid (101955) Bennu's weak boulders and thermally anomalous equator. Sci. Adv. 6 (41), eabc3699.

Rozitis, B., Ryan, A., Emery, J., Nolan, M., Green, S., Christensen, P., Hamilton, V., Daly, M., Barnouin, O., Lauretta, D., 2022. High-resolution thermophysical analysis of the OSIRIS-REx sample site and three other regions of interest on bennu. J. Geophys. Res.: Planets 127 (6), e2021JE007153.

Sasaki, S., Nakamura, K., Hamabe, Y., Kurahashi, E., Hiroi, T., 2001. Production of iron nanoparticles by laser irradiation in a simulation of lunar-like space weathering. Nature 410 (6828), 555–557.

Scheeres, D.J., 2015. Landslides and mass shedding on spinning spheroidal asteroids. Icarus 247, 1–17.

Scheeres, D., French, A., Tricarico, P., Chesley, S., Takahashi, Y., Farnocchia, D., McMahon, J., Brack, D., Davis, A., Ballouz, R.-L., et al., 2020. Heterogeneous mass distribution of the rubble-pile asteroid (101955) Bennu. Sci. Adv. 6 (41), eabc3350.

Scheeres, D., McMahon, J., French, A., Brack, D., Chesley, S., Farnocchia, D., Takahashi, Y., Leonard, J., Geeraert, J., Page, B., et al., 2019. The dynamic geophysical environment of (101955) Bennu based on OSIRIS-REx measurements. Nat. Astron. 3 (4), 352–361.

Schmedemann, N., Kneissl, T., Neesemann, A., Stephan, K., Jaumann, R., Krohn, K., Michael, G., Matz, K.-D., Otto, K., Raymond, C., et al., 2016. Timing of optical maturation of recently exposed material on Ceres. Geophys. Res. Lett. 43 (23), 11–987.

Schröder, S., Mottola, S., Carsenty, U., Ciarniello, M., Jaumann, R., Li, J.-Y., Longobardo, A., Palmer, E., Pieters, C., Preusker, F., et al., 2017. Resolved spectrophotometric properties of the Ceres surface from Dawn Framing Camera images. Icarus 288, 201–225.

Sen, A., Clark, B.E., Cloutis, E.A., DellaGiustina, D.N., Hendrix, A.R., Simon, A.A., Applin, D.M., Parkinson, A., Turenne, N., Connell, S., Ferrone, S.M., Li, J.-Y., Lim, L.F., Lauretta, D.S., 2021b. Spectral effects of varying texture and composition in two-component "mudpie" simulations: Insights for Asteroid (101955) Bennu. Meteorit. Planet. Sci. 56 (6), 1173–1190.

Sen, A., Clark, B.E., Zou, X.-D., Li, J.-Y., Barucci, M., Praet, A., Barker, M., Neumann, G., Mazarico, E., Simon, A., et al., 2021a. Latitude dependence of spectral properties on Bennu: Relevance to space weathering. In: Lunar and Planetary Science Conference, 2548. p. 1538.

Shestopalov, D., Golubeva, L., Cloutis, E., 2013. Optical maturation of asteroid surfaces. Icarus 225 (1), 781–793.

Shimaki, Y., Senshu, H., Sakatani, N., Okada, T., Fukuhara, T., Tanaka, S., Taguchi, M., Arai, T., Demura, H., Ogawa, Y., et al., 2020. Thermophysical properties of the surface of asteroid 162173 Ryugu: Infrared observations and thermal inertia mapping. Icarus 348, 113835.

Simon, A., Kaplan, H., Cloutis, E., Hamilton, V., Lantz, C., Reuter, D., Trang, D., Fornasier, S., Clark, B.E., Lauretta, D., 2020b. Weak spectral features on (101995) Bennu from the OSIRIS-REx Visible and InfraRed Spectrometer. Astron. Astrophys. 644, A148.

Simon, A., Kaplan, H., Hamilton, V., Lauretta, D., Campins, H., Emery, J., Barucci, M., DellaGiustina, D., Reuter, D., Sandford, S., Golish, D., Lim, L., Ryan, A., Rozitis, B., Bennett, C., 2020a. Widespread carbon-bearing materials on near-Earth asteroid (101955) Bennu. Science 370 (6517), eabc3522.

Simon, A.A., Reuter, D.C., Gorius, N., Lunsford, A., Cosentino, R.G., Wind, G., Lauretta, D.S., Team, O.-R., 2018. In-flight calibration and performance of the OSIRIS-REx Visible and IR Spectrometer (OVIRS). Remote Sens. 10 (9), 1486.

Stephan, K., Jaumann, R., Krohn, K., Schmedemann, N., Zambon, F., Tosi, F., Carrozzo, F., McFadden, L., Otto, K., De Sanctis, M., et al., 2017. An investigation of the bluish material on Ceres. Geophys. Res. Lett. 44 (4), 1660–1668.

Stephan, K., Jaumann, R., Zambon, F., Carrozzo, F., Wagner, R., Longobardo, A., Palomba, E., De Sanctis, M., Tosi, F., Ammannito, E., et al., 2019. Ceres' impact craters–Relationships between surface composition and geology. Icarus 318, 56–74.

Sugita, S., Honda, R., Morota, T., Kameda, S., Sawada, H., Tatsumi, E., Yamada, M., Honda, C., Yokota, Y., Kouyama, T., et al., 2019. The geomorphology, color, and thermal properties of Ryugu: Implications for parent-body processes. Science 364 (6437).

Takir, D., Emery, J.P., Mcsween Jr., H.Y., Hibbitts, C.A., Clark, R.N., Pearson, N., Wang, A., 2013. Nature and degree of aqueous alteration in CM and CI carbonaceous chondrites. Meteorit. Planet. Sci. 48 (9), 1618–1637.

Tatsumi, E., Domingue, D., Schröder, S., Yokota, Y., Kuroda, D., Ishiguro, M., Hasegawa, S., Hiroi, T., Honda, R., Hemmi, R., et al., 2020. Global photometric properties of (162173) Ryugu. Astron. Astrophys. 639, A83.

Tatsumi, E., Sakatani, N., Riu, L., Matsuoka, M., Honda, R., Morota, T., Kameda, S., Nakamura, T., Zolensky, M., Brunetto, R., et al., 2021. Spectrally blue hydrated parent body of asteroid (162173) Ryugu. Nature Commun. 12 (1), 5837.

Thomas, P., Robinson, M.S., 2005. Seismic resurfacing by a single impact on the asteroid 433 Eros. Nature 436 (7049), 366–369.

Thomas, C.A., Trilling, D.E., Rivkin, A.S., Linder, T., 2021. Space weathering within C-complex main belt asteroid families. Astron. J. 161 (3), 99.

Thompson, M., Loeffler, M., Morris, R., Keller, L., Christoffersen, R., 2019. Spectral and chemical effects of simulated space weathering of the Murchison CM2 carbonaceous chondrite. Icarus 319, 499–511.

Thompson, M., Morris, R., Clemett, S., Loeffler, M., Trang, D., Keller, L., Christoffersen, R., Agresti, D., 2020. The effect of progressive space weathering on the organic and inorganic components of a carbonaceous chondrite. Icarus 346, 113775.

Trang, D., Lucey, P.G., 2019. Improved space weathering maps of the lunar surface through radiative transfer modeling of Kaguya multiband imager data. Icarus 321, 307–323.

Trang, D., Thompson, M.S., Clark, B.E., Kaplan, H.H., Zou, X.-D., Li, J.-Y., Ferrone, S.M., Hamilton, V.E., Simon, A.A., Reuter, D.C., et al., 2021. The role of hydrated minerals and space weathering products in the bluing of carbonaceous asteroids. Planet. Sci. J. 2 (2), 68.

Vernazza, P., Binzel, R., Rossi, A., Fulchignoni, M., Birlan, M., 2009. Solar wind as the origin of rapid reddening of asteroid surfaces. Nature 458 (7241), 993–995.

Vernazza, P., Fulvio, D., Brunetto, R., Emery, J., Dukes, C., Cipriani, F., Witasse, O., Schaible, M., Zanda, B., Strazzulla, G., et al., 2013. Paucity of tagish lake-like parent bodies in the Asteroid Belt and among Jupiter Trojans. Icarus 225 (1), 517–525.

Walsh, K.J., Ballouz, R.-L., Jawin, E.R., Avdellidou, C., Barnouin, O.S., Bennett, C.A., Bierhaus, E.B., Bos, B.J., Cambioni, S., Connolly Jr., H.C., et al., 2022. Near-zero cohesion and loose packing of Bennu's near subsurface revealed by spacecraft contact. Sci. Adv. 8 (27), eabm6229.

Walsh, K., Jawin, E., Ballouz, R.-L., Barnouin, O., Bierhaus, E., Connolly, H., Molaro, J., McCoy, T., Delbo, M., Hartzell, C., et al., 2019. Craters, boulders and regolith of (101955) Bennu indicative of an old and dynamic surface. Nat. Geosci. 12 (4), 242–246.

Watanabe, S., Hirabayashi, M., Hirata, N., Hirata, N., Noguchi, R., Shimaki, Y., Ikeda, H., Tatsumi, E., Yoshikawa, M., Kikuchi, S., et al., 2019. Hayabusa2 arrives at the carbonaceous asteroid 162173 Ryugu—A spinning top–shaped rubble pile. Science 364 (6437), 268–272.

Watanabe, S.-i., Tsuda, Y., Yoshikawa, M., Tanaka, S., Saiki, T., Nakazawa, S., 2017. Hayabusa2 mission overview. Space Sci. Rev. 208 (1), 3–16.

Willman, M., Jedicke, R., Moskovitz, N., Nesvornỳ, D., Vokrouhlickỳ, D., Mothé-Diniz, T., 2010. Using the youngest asteroid clusters to constrain the space weathering and gardening rate on S-complex asteroids. Icarus 208 (2), 758–772.

Yada, T., Abe, M., Okada, T., Nakato, A., Yogata, K., Miyazaki, A., Hatakeda, K., Kumagai, K., Nishimura, M., Hitomi, Y., et al., 2022. Preliminary analysis of the Hayabusa2 samples returned from C-type asteroid Ryugu. Nat. Astron. 6 (2), 214–220.

Yokota, Y., Honda, R., Tatsumi, E., Domingue, D., Schröder, S., Matsuoka, M., Morota, T., Sakatani, N., Kameda, S., Kouyama, T., et al., 2021. Opposition observations of 162173 Ryugu: Normal albedo map highlights variations in regolith characteristics. Planet. Sci. J. 2 (5), 177.

Zou, X.-D., Li, J.-Y., Clark, B.E., Golish, D.R., Ferrone, S., Simon, A.A., Reuter, D.C., Domingue, D.L., Kaplan, H., Barucci, M.A., et al., 2021. Photometry of asteroid (101955) Bennu with OVIRS on OSIRIS-REx. Icarus 358, 114183.